Revisiting the State-of-Charge Estimation for Lithium-Ion Batteries

A METHODICAL INVESTIGATION OF THE EXTENDED KALMAN FILTER APPROACH

YEBIN WANG, HUAZHEN FANG, LEI ZHOU, and TOSHIHIRO WADA

IMAGE COURTESY OF HUAZHEN FANG

With high energy/power density, flexible and lightweight design, low self-discharge rates and long cycle life, lithium-ion (Li^+) batteries have experienced a surging growth since being commercialized in the early 1990s [1]. They are dominant today in the consumer electronics sector. Due to continually declining manufacturing costs, they are also rapidly penetrating sectors such as the power grid, renewable energy, automotive, and aerospace, where large-scale energy storage is needed. Looking into the future, the role of Li^+ batteries will be further strengthened as a key energy-storage technology to support the progression of the world into the green energy era. However, their vulnerability to overcharge, overdischarge, and overheating can easily expose them to performance degradation, shortened cycle life, and even fire and explosion, thus raising many concerns about their deployment. These challenges have been driving a massive solution-seeking effort in various relevant research fields. Associated with this trend is the control-theory-enabled advancement of battery-management system (BMS) technologies.

A BMS monitors the states and parameters of batteries; regulates the charging/discharging processes; and performs balancing across battery cells to meet the power demands, enhance safety and performance, and extend

Digital Object Identifier 10.1109/MCS.2017.2696761
Date of publication: 18 July 2017

1066-033X/17©2017IEEE

battery lifespan. Among the tasks, state-of-charge (SoC) monitoring is particularly important. Representing the amount of charge remaining in a battery, the SoC cannot be directly measured but is crucial for preventing overcharge and overdischarge, which has stimulated an ongoing quest for high-caliber estimation strategies. Nevertheless, the evolution of SoC through time is based on complex nonlinear dynamic processes arising from thermodynamics, electrode kinetics, and transport phenomena. As a result, SoC monitoring involves, at its core, solving nonlinear estimation problems and has been actively researched in the last decade. An overview of the state of the art is presented in "Survey of State-of-Charge Estimation."

This article presents a self-contained study of the SoC estimation problem for Li^+ batteries and solutions based on the extended Kalman filter (EKF). The EKF, reviewed in "Extended Kalman Filter," is arguably the most celebrated nonlinear estimation approach, and its popularity has extended to battery management research to the point that it is now widely acknowledged in the literature as one of the best techniques for SoC estimation. Its application to this subject, however, is not conclusive yet. The present literature has focused more on the use of the EKF technique, with less emphasis on the observability and sensitivity analysis crucial for successful estimation. The consequence is that some potential problems or pitfalls can escape notice—for instance, some unknown and weakly observable parameters can potentially compromise the accuracy of the full-state estimation without being detected. To remedy this issue, this study takes an analysis-driven perspective and systematically demonstrates how nonlinear estimation theory can be effectively used to understand the risks and challenges underlying accurate SoC estimation and to build insights into improving the prevailing estimation methods.

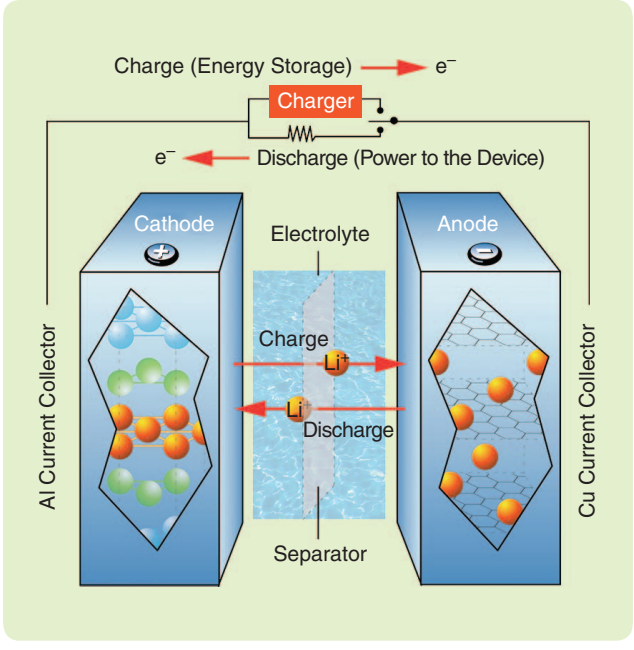

FIGURE 1 A schematic for a Li^+ battery. A Li^+ battery cell consists of four major components: the negative electrode (anode), positive electrode (cathode), electrolyte, and separator. Both electrodes comprise small particles filled with active material. During charge or discharge, a reduction-oxidation reaction occurs at particles of one electrode and leads to the release of Li^+ ions into the electrolyte. The Li^+ ions are then transported to the other electrode, where they are absorbed into particles. (Image courtesy of Argonne National Laboratory.)

With a brief description of Li^+ battery fundamentals and modeling, a thorough observability and sensitivity analysis is performed to illustrate the potential pitfalls that may fundamentally undermine the effectiveness of SoC estimation. Specifically, it is found that adaptive SoC estimation can be susceptible to a fundamental limitation plaguing adaptive systems: weak observability due to overparameterized models and insufficiently informative data. Building on the observability/sensitivity analysis, the notion of parameter subset selection is leveraged to identify critical parameters; thus, the weak observability and numerical stability issues are circumvented. Accordingly, a new enhanced adaptive SoC estimator, consisting of two reduced-order EKFs running in the cascade mode, is developed. Additionally, a two-stage EKF is presented to reduce the computational cost of the joint EKF-based SoC estimator. All estimators are validated by synthetic and/or experimental data. The validation results agree with the outcomes drawn from the analysis. This article is concluded by a summary and an outlook to future work.

Li^+ BATTERIES AND MODELING

Preliminaries of Li^+ Batteries

This section briefly overviews the characteristics and modeling of Li^+ batteries (see [2]–[8] for more details). A schematic description of a Li^+ battery cell is shown in Figure 1. The cell is composed of four main elements: the positive electrode, negative electrode, electrolyte, and separator. The positive electrode is typically made from Li^+ compounds, for instance, $LiFePO_4$, $Li_xMn_2O_4$, or Li_xCoO_2. Small solid particles of the compounds are compressed together, yielding a porous structure. The negative electrode is porous as well but usually made of carbon or graphite particles. The interstitial pores at both electrodes offer intercalation space, where the Li^+ ions can be moved in and out for storage and release. The electrolyte contains free ions and is electrically conductive, in which the Li^+ ions can be transported easily. The separator, separating the electrodes apart, allows the migration of Li^+ ions from one side to the other but prevents electrons from passing through. The electrons are thus forced to flow through the external circuit. During the charging process, Li^+ ions are released from particles at the positive electrode into the electrolyte and then transported to and stored in the negative electrode.

This process not only generates an influx of Li^+ ions within the battery but also builds up a potential difference between the positive and negative electrodes. Discharging is based on the reversed process. The chemical reactions in the positive and negative electrodes of a $LiFePO_4/C$ battery are exemplified by

$$LiFePO_4 \underset{\text{discharge}}{\overset{\text{charge}}{\rightleftharpoons}} FePO_4 + Li^+ + e^-, \tag{1}$$

$$Li^+ + e^- + C_6 \underset{\text{discharge}}{\overset{\text{charge}}{\rightleftharpoons}} LiC_6. \tag{2}$$

The working mechanism (1)–(2) has been naturally abstracted through electrochemical principles into a diversity of two-dimensional (2-D) electrochemical models, among which are the Doyle–Fuller–Newman model and its variants [2], [3], [9]. These models can provide a high-fidelity characterization of the underlying physical and chemical processes, which makes them suitable for battery design and analysis. However, they are rarely adopted in real-time BMSs, largely due to their prohibitive computation and onerous calibration. This weakness has been significantly relaxed by the single-particle model (SPM) and its extensions [5], [8], [10], [11], which simplify the 2-D electrochemical models to one spatial dimension. Specifically, the SPM is derived by neglecting the electrolyte dynamics and treating each electrode as a spherical particle that stores Li^+. The SPM is valid for low to medium charge/discharge currents (up to 1 C-rate) [5], [8]. While the SPM enjoys remarkable reduction of computation and calibration efforts in contrast to the 2-D electrochemical models, it remains computationally expensive for real-time battery management with a representation based on partial differential equations (PDEs).

Instead of using the electrochemical principles, many other approaches to battery models have been developed to meet different needs. In particular, equivalent circuit models (ECMs) with their simplicity have gained wide popularity among control engineers, representing a model class most useful for BMS design and implementation [6], [7], [12]–[14]. ECMs are intended to replicate the battery's input–output characteristics or, in other words, emulate how charge/discharge currents influence the terminal voltage. A straightforward tool to understand and deduce the ECMs is Thévenin's theorem in circuit theory. A Thévenin-based model consists of a series resistor, a resistor-capacitor (RC) circuit, and a voltage source and has been found capable of predicting the transient response of the battery with sufficient accuracy. See [7], [13], and [14] for comparative studies of various ECMs. Overall, ECMs are among the most advantageous for embedded BMS development and will serve as a basis for SoC estimation in this article.

This article defines the terminology from a user's perspective, treating the battery as an electric power source. The battery is considered to be fully charged and discharged when, with small charge and discharge currents, its terminal voltage reaches certain upper and lower thresholds. For the $LiFePO_4$-type cell used in our experiment (to be presented later), it reaches full charge or discharge if its terminal voltage crosses 4.2 and 2.4 V. A battery's nominal capacity is the amount of charge that it can take when brand new. The maximum capacity is the amount of charge that can be extracted from a fully charged battery. The SoC represents the energy available in a battery. Typically quantified by the ratio between the remaining amount of charge and the maximum capacity, the SoC takes values in $[0,1]$. The state of health (SoH) indicates the fading of the battery's maximum capacity. The SoH level will decrease gradually throughout the charge and discharge cycles. In general understanding, the capacity fading is attributed to unwanted side reactions including electrolyte decomposition, active material dissolution, and passive film formation. The open-circuit voltage (OCV) is the terminal voltage of the battery when it is cut off from the load. The OCV is uniquely determined by the SoC because the OCV corresponds to the difference between electrostatic potentials of the negative and positive electrodes, and the electrostatic potential of an electrode is determined by the quantities of Li^+ ions stored in the electrode [8]. The SoC-OCV curve of the battery cell used in the experiment is shown in Figure 2 as the red dash-dot line.

Batteries have many interesting but complicated phenomena such as capacity fading, self-discharge, relaxation,

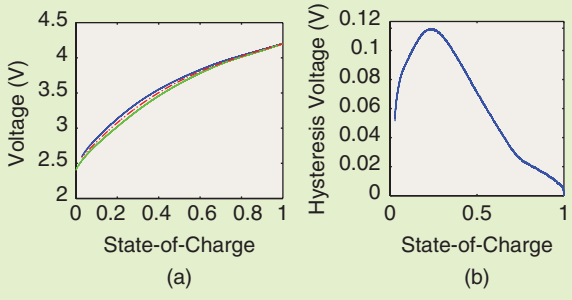

FIGURE 2 State-of-charge (SoC) versus terminal voltage curves during discharge and charge processes. (a) The terminal voltages while the battery is charged and discharged with a current 0:235 A. Blue solid line: the terminal voltage during the charge process (the charge curve); green solid line: the terminal voltage during the discharge process (the discharge curve); red dash-dot line: the SoC versus open circuit voltage curve obtained by averaging the discharge and charge curves. (b) The hysteresis between the charge and discharge curves. In battery model (3), the hysteresis in the charge and discharge curves is captured by the series resistance, the RC circuit, and the hysteresis voltage x^3. Since the resistances are on the order of milliohms and the amplitude of currents is small, the voltages across the series resistor and the RC circuit are negligible compared with x^3. The influence of temperature on the hysteresis is also suppressed by maintaining ambient temperature during the test. The SoC is obtained from the Coulomb counting method. The hysteresis voltage is SoC dependent.

Survey of State-of-Charge Estimation

Li^+ batteries are widely recognized as a key enabler for the worldwide migration toward clean and sustainable energy supply, with tremendous application in the sectors of transportation, aerospace, buildings, renewables, and smart grid. Due to the materials used and the electrochemistries, they are, however, vulnerable to overcharge and overdischarge, which can cause fast aging and even cause fires and explosions in extreme cases. Accurate SoC estimation thus becomes a necessity to avoid such issues and, furthermore, provide a foundation of support for other higher-level battery management tasks. Depending on the explicit use of a battery model or not, existing SoC estimation methods can be divided into two categories, *model based* and *nonmodel based*, an current review of which is offered below.

Conventional model-free methods are based on measuring or calculating certain parameters directly linked with the SoC. Two straightforward, yet representative, methods in this regard are voltage translation and Coulomb counting [S1]. The former infers the SoC from a predetermined OCV-SoC lookup table using the OCV measurement. Although reliable, this method requires the battery to rest for a long time cut off from the external circuit to measure the OCV. Coulomb counting is based on numerical integration of the current over time. It is easy to implement but can suffer from a "drift" from the true values due to cumulative integration errors and noise corruption. These methods have still gained much popularity because of their simplicity and convenience. They are also integrated with model-based methods in some recent developments for improved SoC estimation; see [S2] and [S3]. Another class of model-free SoC estimation methods are based on machine learning. Without requiring an ECM or electrochemical model, they train the battery data sets to build an abstract mathematical description to approximate the battery behavior and then estimate the SoC. The main tools that have been used include artificial neural networks [S4]–[S7] and a support vector machine [S8]–[S11]. With sights set on data-driven inference and reasoning, machine learning offers a useful means of mining the battery operation data collected over time for SoC monitoring and more tasks. The training, however, can be complex and may imply much preparatory work before the algorithm deployment. In addition, the neural-network computation can be costly and thus unsuitable for onboard/embedded application.

Given the availability of a diverse range of battery models, recent years have seen a shift of attention toward model-based SoC estimation methods, which can offer improved accuracy while allowing real-time execution. This research front, at the nexus of Li^+ battery systems and estimation theory, is expanding rapidly, with a large body of work published. Results based on both ECMs and electrochemical models have been widely reported. The equivalent-circuit-based models generally offer a low-complexity description of the Li^+ battery dynamics with fewer states and parameters, and thus are conducive to fast SoC estimation. The electrochemical models, in the form of PDEs, represent a more sophisticated view of the battery dynamics while often requiring more computational or model reduction effort.

From the perspective of estimation, the existing literature puts two types of approaches into use: stochastic estimation and nonlinear observers. For the former type, the KF is in a leading position. Many KF techniques, including the EKF, iterated EKF, and sigma-point KF, have been applied to different SoC problem settings or battery models [16], [17], [S12]–[S27]. Another avenue builds on the particle filtering (PF) technique, which is capable of handling severe nonlinearities and non-Gaussian noise; see [S28]–[S31]. The stochastic estimation approach has emerged as a natural choice, primarily for its ability to suppress the noise affecting a battery system. Its appeal is further enhanced by the applicability to general nonlinear systems and thus almost every battery model. When it comes to computational efficiency, KFs are competitive, especially when used for a low-dimensional battery model, as often needed for real-world implementation. The PFs, by contrast, demand more computational resources. Although the convergence properties of these methods can be difficult to analyze due to nonlinearities and noise, the above merits have still made them among the most favored choices in practice. The second type of model-based methods, called nonlinear SoC observers, has also drawn a lot of interest in the past several years. The present literature now covers a broad range of design techniques, including the Luenberger observer [S1], [S32], adaptive observer [S33]–[S38], sliding-mode observer [S39]–[S42], output-injection PDE observer [S43]–[S45], backstepping PDE observer [S46], and robust nonlinear observer [S47]. The SoC observers proceed on the premise that the battery system is at least approximately deterministic. Though restrictive to some extent, the deterministic assumption eliminates the need for maintaining covariance matrices and thus enables higher computational efficiency of SoC estimation. The observer approach, while enjoying application to ECMs, is also suitable for some PDE-based battery models such as the single-particle model.

REFERENCES

[S1] C. D. Rahn and C.-Y. Wang, *Battery Management Systems*. Hoboken, NJ: Wiley, 2013, pp. 191–229.

[S2] F. Codeca, S. M. Savaresi, and G. Rizzoni, "On battery state of charge estimation: A new mixed algorithm," in *Proc. IEEE Int. Conf. Control Applications*, 2008, pp. 102–107.

[S3] M. Verbrugge and E. Tate, "Adaptive state of charge algorithm for nickel metal hydride batteries including hysteresis phenomena," *J. Power Sources*, vol. 126, no. 1, pp. 236–249, 2004.

[S4] M. Charkhgard and M. Farrokhi, "State-of-charge estimation for lithium-ion batteries using neural networks and EKF," *IEEE Trans. Ind. Electron.*, vol. 57, no. 12, pp. 4178–4187, 2010.

[S5] C.-H. Cai, D. Dong, Z.-Y. Liu, and H. Zhang, "Artificial neural network in estimation of battery state of-charge (SOC) with nonconventional input variables selected by correlation analysis," in *Proc. Int. Conf. Machine Learning and Cybernetics*, 2002, vol. 3, pp. 1619–1625.

[S6] A. Affanni, A. Bellini, C. Concari, G. Franceschini, E. Lorenzani, and C. Tassoni, "EV battery state of charge: neural network based estimation," in *Proc. IEEE Int. Electric Machines and Drives Conf.*, 2003, vol. 2, pp. 684–688.
[S7] G. W. W. L. Bi Jun, and S. Sai, "State of charge estimation of Li-ion batteries in electric vehicle based on radial-basis-function neural network," *Chin. Phys. B*, vol. 21, no. 11, pp. 118801, 2012.
[S8] J. Hu, J. Hu, H. Lin, X. Li, C. Jiang, X. Qiu, and W. Li, "State-of-charge estimation for battery management system using optimized support vector machine for regression," *J. Power Sources*, vol. 269, pp. 682–693, Dec. 2014.
[S9] J. C. A. Anton, P. J. G. Nieto, C. B. Viejo, and J. A. V. Vilan, "Support vector machines used to estimate the battery state of charge," *IEEE Trans. Power Electron.*, vol. 28, no. 12, pp. 5919–5926, 2013.
[S10] Q. S. Shi, C. H. Zhang, and N. X. Cui, "Estimation of battery state-of-charge using v-support vector regression algorithm," *Int. J. Automot. Technol.*, vol. 9, no. 6, pp. 759–764, 2008.
[S11] T. Hansen and C.-J. Wang, "Support vector based battery state of charge estimator," *J. Power Sources*, vol. 141, no. 2, pp. 351–358, 2005.
[S12] D. Di Domenico, A. Stefanopoulou, and G. Fiengo, "Lithium-ion battery state of charge and critical surface charge estimation using an electrochemical model-based extended Kalman filter," *J. Dyn. Syst. Meas. Control*, vol. 132, no. 6, p. 061302, 2010.
[S13] H. Fang, Y. Wang, Z. Sahinoglu, T. Wada, and S. Hara, "State of charge estimation for lithium-ion batteries: An adaptive approach," *Control Eng. Pract.*, vol. 25, pp. 45–54, Apr. 2014.
[S14] H. Fang, X. Zhao, Y. Wang, Z. Sahinoglu, T. Wada, S. Hara, and R. A. de Callafon, "Improved adaptive state-of-charge estimation for batteries using a multi-model approach," *J. Power Sources*, vol. 254, pp. 258–267, May 2014.
[S15] Y. Zou, X. Hu, H. Ma, and S. E. Li, "Combined state of charge and state of health estimation over lithium-ion battery cell cycle lifespan for electric vehicles," *J. Power Sources*, vol. 273, pp. 793–803, Jan. 2015.
[S16] J. Lee, O. Nam, and B. Cho, "Li-ion battery SOC estimation method based on the reduced order extended Kalman filtering," *J. Power Sources*, vol. 174, no. 1, pp. 9–15, 2007.
[S17] J. Han, D. Kim, and M. Sunwoo, "State-of-charge estimation of lead-acid batteries using an adaptive extended Kalman filter," *J. Power Sources*, vol. 188, no. 2, pp. 606–612, 2009.
[S18] O. Barbarisi, F. Vasca, and L. Glielmo, "State of charge Kalman filter estimator for automotive batteries," *Control Eng. Pract.*, vol. 14, no. 3, pp. 267–275, 2006.
[S19] S. Santhanagopalan and R. E. White, "State of charge estimation using an unscented filter for high power lithium ion cells," *Int. J. Energy Res.*, vol. 34, no. 2, pp. 152–163, 2010.
[S20] G. L. Plett, "Sigma-point Kalman filtering for battery management systems of LiPB-based HEV battery packs: Part 2: Simultaneous state and parameter estimation," *J. Power Sources*, vol. 161, no. 2, pp. 1369–1384, 2006.
[S21] S. Pang, J. Farrell, D. Jie, and M. Barth, "Battery state-of-charge estimation," in *Proc. American Control Conf.*, 2001, vol. 2, pp. 1644–1649.
[S22] C. Weng, J. Sun, and H. Peng, "A unified open-circuit-voltage model of lithium-ion batteries for state-of-charge estimation and state-of-health monitoring," *J. Power Sources*, vol. 258, pp. 228–237, July 2014.
[S23] K. Smith, C. Rahn, and C.-Y. Wang, "Model-based electrochemical estimation and constraint management for pulse operation of lithium ion batteries," *IEEE Trans. Control Syst. Technol.*, vol. 18, no. 3, pp. 654–663, 2010.
[S24] R. Xiong, X. Gong, C. C. Mi, and F. Sun, "A robust state-of-charge estimator for multiple types of lithium-ion batteries using adaptive extended Kalman filter," *J. Power Sources*, vol. 243, pp. 805–816, Dec. 2013.
[S25] A. Bizeray, S. Zhao, S. Duncan, and D. Howey, "Lithium-ion battery thermal-electrochemical model-based state estimation using orthogonal collocation and a modified extended Kalman filter," *J. Power Sources*, vol. 296, pp. 400–412, Nov. 2015.
[S26] C. Taborelli and S. Onori, "State of charge estimation using extended Kalman filters for battery management system," in *Proc. IEEE Int. Electric Vehicle Conf.*, 2014, pp. 1–8.
[S27] X. Lin, A. Stefanopoulou, P. Laskowsky, J. Freudenberg, Y. Li, and R. Dyche, "State of charge estimation error due to parameter mismatch in a generalized explicit lithium ion battery model," in *Proc. ASME Dynamic Systems and Controls Conf.*, 2011, pp. 393–400.
[S28] A. Bartlett, J. Marcicki, S. Onori, G. Rizzoni, X. G. Yang, and T. Miller, "Electrochemical model-based state of charge and capacity estimation for a composite electrode lithium-ion battery," *IEEE Trans. Control Syst. Technol.*, vol. 24, no. 2, pp. 384–399, 2016.
[S29] Y. Wang, C. Zhang, and Z. Chen, "A method for state-of-charge estimation of LiFePO4 batteries at dynamic currents and temperatures using particle filter," *J. Power Sources*, vol. 279, pp. 306–311, Apr. 2015.
[S30] M. F. Samadi, S. M. M. Alavi, and M. Saif, "Online state and parameter estimation of the Li-ion battery in a Bayesian framework," in *Proc. American Control Conf.*, 2013, pp. 4693–4698.
[S31] R. Restaino and W. Zamboni, "Comparing particle filter and extended Kalman filter for battery state-of-charge estimation," in *Proc. 38th Annu. Conf. IEEE Industrial Electronics Society*, 2012, pp. 4018–4023.
[S32] Q. Ouyang, J. Chen, F. Wang, and H. Su, "Nonlinear observer design for the state of charge of lithium-ion batteries," in *Proc. 9th World Congress Int. Federation Automatic Control*, 2014, pp. 2794–2799.
[S33] Y. Wang, H. Fang, Z. Sahinoglu, T. Wada, and S. Hara, "Adaptive estimation of the state of charge for lithium-ion batteries: Nonlinear geometric observer approach," *IEEE Trans. Control Syst. Technol.*, 2015, in press.
[S34] Y. Wang, H. Fang, Z. Sahinoglu, T. Wada, and S. Hara, "Nonlinear adaptive estimation of the state of charge for lithium-ion batteries," in *Proc. IEEE Conf. Decision Control*, 2013, pp. 4405–4410.
[S35] M. El Lakkis, O. Sename, M. Corno, and D. Bresch Pietri, "Combined battery SOC/SOH estimation using a nonlinear adaptive observer," in *Proc. European Control Conf.*, 2015, pp. 1522–1527.
[S36] L. Liu, L. Y. Wang, Z. Chen, C. Wang, F. Lin, and H. Wang, "Integrated system identification and state-of-charge estimation of battery systems," *IEEE Trans. Energy Convers.*, vol. 28, no. 1, pp. 12–23, 2013.
[S37] S. Dey, B. Ayalew, and P. Pisu, "Nonlinear adaptive observer for a lithium-ion battery cell based on coupled electrochemical-thermal model," *ASME J. Dyn. Syst. Meas. Control*, vol. 137, no. 11, p. 111005, 2014.
[S38] Y. Li, R. D. Anderson, J. Song, A. M. Phillips, and X. Wang, "A nonlinear adaptive observer approach for state of charge estimation of lithium-ion batteries," in *Proc. American Control Conf.*, 2011, pp. 370–375.
[S39] I.-S. Kim, "The novel state of charge estimation method for lithium battery using sliding mode observer," *J. Power Sources*, vol. 163, no. 1, pp. 584–590, 2006.
[S40] A. Belhani, N. K. M'Sirdi, and A. Naamane, "Adaptive sliding mode observer for estimation of state of charge," *Energy Proc.*, vol. 42, pp. 377–386, Jan. 2013.
[S41] X. Chen, W. Shen, Z. Cao, A. Kapoor, and I. Hijazin, "Adaptive gain sliding mode observer for state of charge estimation based on combined battery equivalent circuit model in electric vehicles," in *Proc. IEEE 8th Conf. Industrial Electronics and Applications*, 2013, pp. 601–606.
[S42] F. Zhang, G. Liu, and L. Fang, "A battery state of charge estimation method using sliding mode observer," in *Proc. 7th World Congress on Intelligent Control and Automation*, 2008, pp. 989–994.
[S43] S. J. Moura, N. A. Chaturvedi, and M. Krstic, "PDE estimation techniques for advanced battery management systems—Part i: Soc estimation," in *Proc. American Control Conf.*, 2012, pp. 559–565.
[S44] S. J. Moura, N. A. Chaturvedi, and M. Krstić, "Adaptive partial differential equation observer for battery state-of-charge/state-of-health estimation via an electrochemical model," *ASME J. Dyn. Syst. Meas. Control*, vol. 136, no. 1, pp. 011 015–011 015–11, 2013.
[S45] R. Klein, N. Chaturvedi, J. Christensen, J. Ahmed, R. Findeisen, and A. Kojic, "Electrochemical model based observer design for a Lithium-ion battery," *IEEE Trans. Control Syst. Technol.*, vol. 21, no. 2, pp. 289–301, 2013.
[S46] S. Tang, Y. Wang, Z. Sahinoglu, T. Wada, S. Hara, and M. Krstic, "State-of-charge estimation for lithium-ion batteries via a coupled thermal-electrochemical model," in *Proc. American Control Conf.*, 2015, pp. 5871–5877.
[S47] N. Lotfi and R. Landers, "Robust nonlinear observer for state of charge estimation of Li-ion batteries," in *Proc. ASME Dynamic Systems Controls Conf.*, 2012, pp. 15–20.

Extended Kalman Filter

A dynamic system subjected to the effects of noise is referred to as a stochastic dynamic system [S48], which is present in almost every engineering field. With the inclusion of noise, a stochastic system can behave significantly differing from its deterministic counterpart. A significant research effort has thus been stimulated, since the seminal work by Einstein [S49], to investigate such systems, including their behavior characterization, control, and estimation. Because it is practically infeasible to measure each state of a stochastic system, unknown state estimation has been undergoing several decades of active research. In this research field, the Kalman filtering techniques have established a lead, and in particular, the EKF has emerged as the most celebrated estimation tool for nonlinear stochastic systems. A brief overview of this technique is given below. Consider the model

$$\begin{aligned} x_{k+1} &= f(x_k) + w_k, \\ y_k &= h(x_k) + v_k, \end{aligned} \tag{S1}$$

where $x_k \in \mathbb{R}^{n_x}$ is the unknown system state, $y_k \in \mathbb{R}^{n_y}$ the output, and $\{w_k\}$ and $\{v_k\}$ are noise sequences assumed to be Gaussian and white, with covariances of Q and R, respectively. The nonlinear mappings $f: \mathbb{R}^{n_x} \to \mathbb{R}^{n_x}$ and $h: \mathbb{R}^{n_x} \to \mathbb{R}^{n_y}$ represent, respectively, the process and measurement models. The EKF produces the estimate of x_k sequentially through time when the measurement y_k becomes available. It consists of two steps, prediction and update. The one-step-forward prediction yields the estimate of x_k, denoted as $\hat{x}_{k|k-1}$, using the measurements collected up to time $k-1$. Then, upon the arrival of y_k, $\hat{x}_{k|k-1}$ will be updated to $\hat{x}_{k|k}$ leveraging the information conveyed by y_k about x_k. In the meantime, the estimation-error covariances associated with both estimates are computed accordingly.

When the state estimate $\hat{x}_{k-1|k-1}$ is generated, consider the first-order Taylor expansion of $f(x_{k-1})$ at this point

$$f(x_{k-1}) \approx f(\hat{x}_{k-1|k-1}) + F_{k-1}(x_{k-1} - \hat{x}_{k-1|k-1}), F_{k-1} = \frac{\partial f}{\partial x}\bigg|_{\hat{x}_{k-1|k-1}}. \tag{S2}$$

A one-step-forward prediction can be made through

$$\hat{x}_{k|k-1} = f(\hat{x}_{k-1|k-1}), \tag{S3}$$

$$P_{k|k-1} = F_{k-1} P_{k-1|k-1} F_{k-1}^{\top} + Q, \tag{S4}$$

where $P_{k|k-1}$ is the prediction-error covariance quantifying the uncertainty of $\hat{x}_{k|k-1}$. After $\hat{x}_{k|k-1}$ is produced, it will be of interest to investigate the updated state estimate. When the new measurement y_k becomes available, the update step can be performed as follows:

$$\hat{x}_{k|k} = \hat{x}_{k|k-1} + \underbrace{P_{k|k-1} H_k^{\top} (H_k P_{k|k-1} H_k^{\top} + R)^{-1}}_{\text{Kalman gain}} [y_k - h(\hat{x}_{k|k-1})], \tag{S5}$$

$$P_{k|k} = P_{k|k-1} - P_{k|k-1} H_k^{\top} (H_k P_{k|k-1} H_k^{\top} + R)^{-1} H_k P_{k|k-1}, \tag{S6}$$

where H_k is obtained by linearization of $h(x_k)$, that is,

$$H_k = \frac{\partial h}{\partial x}\bigg|_{\hat{x}_{k|k-1}}.$$

The EKF then consists of (S3)–(S4) for prediction and (S5)–(S6) for update. The EKF addresses the nonlinearities through linearization of the system functions and then adapts the linear KF to the linearization. A schematic diagram of the EKF is shown in Figure S1.

Since the 1960s, the EKF has gained wide use in the areas of aerospace; robotics; and biomedical, chemical, electrical, and civil engineering and has achieved notable success in numerous real-world applications. This is often ascribed to its conceptual straightforwardness as an extension of the linear KF and, consequently, its relative ease of design and execution. Another important reason is its good convergence from a theoretical viewpoint. In spite of linearization-induced errors, the EKF has provable stability under some conditions that can be satisfied by many practical systems; see [S51]–[S54]. However, the EKF also suffers from some shortcomings. The foremost is the inadequacy of its first-order accuracy for highly

hysteresis, the SoC-OCV relationship, and current-voltage characteristics. Self-discharge represents the fact that the remaining charge stored in a battery will deplete over time. Depending on the cell chemistry, self-discharge could take up to years [4]. Relaxation is the change of the terminal voltage after the battery is disconnected from the load. The relaxation effect results from the Li^+ diffusion that continues even after the cell is cut off from the external circuit and can take up to hours. The hysteresis is generally referred to the phenomenon that during a discharge, the battery terminal voltage always relaxes to a value lower than the true OCV, and during a charge, the battery terminal voltage always relaxes to a value greater than the true OCV [6]. Figure 2 shows the hysteresis effect of the battery cell used in the experiment. Note that batteries with different chemistry could have these characteristics at different levels.

An Equivalent Circuit Model

This article considers the battery model shown in Figure 3. It combines the Thévenin-based ECM [7] with the hysteresis voltage dynamics [6]. The former offers a grasp of dynamic current-voltage characteristics, and the latter compensates the static current-voltage property. The model, striking an adequate balance between fidelity and simplicity, is given by

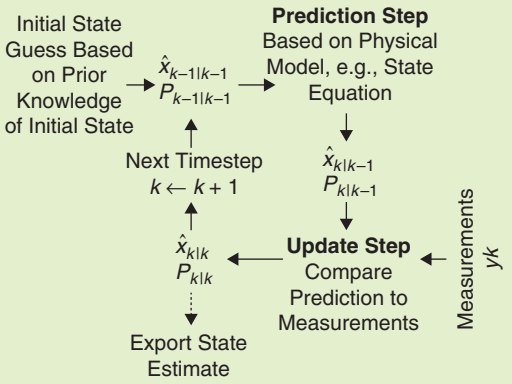

FIGURE S1 A schematic structure of the extended Kalman filter (EKF), modified from [S50]. The EKF comprises two steps sequentially executed through time—prediction and update. For prediction, look at x_k at time $k-1$. The forecast is denoted as $\hat{x}_{k|k-1}$ and subject to uncertainty quantified by the prediction-error covariance $P_{k|k-1}$. The update step occurs upon the arrival of the new measurement y_k. In this step, y_k is leveraged to correct $\hat{x}_{k|k-1}$ and produce the updated estimate $\hat{x}_{k|k}$. Meanwhile, $P_{k|k-1}$ is updated to generate $P_{k|k}$ to quantify the uncertainty imposed on $\hat{x}_{k|k}$.

nonlinear systems. In addition, the need for explicit derivative matrices not only renders the EKF inapplicable for discontinuous or other nondifferentiable systems, but sometimes makes it difficult to program and debug, especially for systems with complex nonlinear functions. This linearity, together with the computational complexity of $O(n_x^3)$, limits the application of EKFs mostly to low-dimensional systems. It should be pointed out, however, that most practical systems are not that complicated in terms of either dimension and nonlinearities and thus can typically be simplified without much loss of model integrity. As a result, the EKF can be applied effectively to a large number of estimation problems, thus it is widely regarded as the most popular estimation technique.

Modified EKFs have also been developed for improved accuracy or efficiency in the past years. In this regard, a natural extension is through the second-order Taylor expansion, which will lead to the second-order EKF with more accurate estimation [S55]–[S57]. Another important variant, called *iterated EKF*, iteratively refines the state estimate around the current point at each time instant [S58], [S59]. Though coming at the expense of an increased computational cost, it can achieve higher estimation accuracy even when severe nonlinearities are present in systems.

REFERENCES

[S48] A. Longtin, "Stochastic dynamical systems," *Scholarpedia*, vol. 5, no. 4, pp. 1619, 2010. doi: 10.4249/scholarpedia.1619.

[S49] A. Einstein, "On the movement of small particles suspended in stationary liquids required by the molecular-kinetic theory of heat," *Ann. Physik*, vol. 17, no. 4, pp. 549–560, 1905.

[S50] Wikipedia. (2016, Apr. 20). Kalman filter. [Online]. Available: https://en.wikipedia.org/wiki/Kalman_filter

[S51] M. Boutayeb, H. Rafaralahy, and M. Darouach, "Convergence analysis of the extended Kalman filter used as an observer for nonlinear deterministic discrete-time systems," *IEEE Trans. Automat. Control*, vol. 42, no. 4, pp. 581–586, 1997.

[S52] A. Krener, "The convergence of the extended Kalman filter," in *Directions in Mathematical Systems Theory and Optimization*, A. Rantzer and C. Byrnes, Eds. New York: Springer-Verlag, 2003, vol. 286, pp. 173–182.

[S53] S. Kluge, K. Reif, and M. Brokate, "Stochastic stability of the extended Kalman filter with intermittent observations," *IEEE Trans. Automat. Control*, vol. 55, no. 2, pp. 514–518, 2010.

[S54] S. Bonnabel and J.-J. Slotine, "A contraction theory-based analysis of the stability of the deterministic extended Kalman filter," *IEEE Trans. Automat. Control*, vol. 60, no. 2, pp. 565–569, 2015.

[S55] H. Tanizaki, *Nonlinear Filters: Estimation and Applications*. Berlin Heidelberg: Springer-Verlag, 1996.

[S56] S. Särkkä, *Bayesian Filtering and Smoothing*. Cambridge, U.K.: Cambridge Univ. Press, 2013.

[S57] M. Roth and F. Gustafsson, "An efficient implementation of the second order extended Kalman filter," in *Proc. 14th Int. Conf. Information Fusion*, 2011, pp. 1–6.

[S58] A. H. Jazwinski, *Stochastic Processes and Filtering Theory*. New York: Academic, 1970.

[S59] B. Bell and F. Cathey, "The iterated Kalman filter update as a Gauss-Newton method," *IEEE Trans. Automat. Control*, vol. 38, no. 2, pp. 294–297, 1993.

$$
\begin{aligned}
\dot{x}^1 &= -\alpha I,\\
\dot{x}^2 &= -\frac{1}{R_d C_d}x^2 + \frac{I}{C_d},\\
\dot{x}^3 &= -\gamma |I| \left[\operatorname{sign}(I) V_{hs}(x^1) + x^3\right],\\
y &= h(x^1) - x^2 + x^3 - R_s I,
\end{aligned} \tag{3}
$$

where x^1 is the SoC, x^2 the voltage cross the RC circuit, x^3 the hysteresis voltage, I the current in discharging ($I > 0$) or charging ($I < 0$), y the terminal voltage, $V_{hs}(x^1)$ the equilibrium of the hysteresis voltage dynamics, and $h(x^1)$ represents the SoC-OCV relationship. The model (3) includes parameters α, R_d, C_d, R_s, and γ, where $\alpha = 1/(3600C_0)$ with C_0 the maximum capacity, γ is the inverse of the hysteresis voltage dynamics time constant, and R_s, R_d, and C_d are as defined in Figure 3. The function $\operatorname{sign}(I) = 1$ for $I \geq 0$ and -1 otherwise. Here, the self-discharge phenomenon is not considered to have a negligible influence because its dynamics are much slower than the dynamics of x^1, x^2, and x^3. The capacity fading can be reflected by the change in α. However, it is also a slow process, at a rate several orders of magnitude smaller than the battery state evolution, which implies that α can be treated as a constant during the SoC estimation. The thermal effects are not explicitly included in battery model (3), but their effects can arguably be compensated by adjusting model parameters.

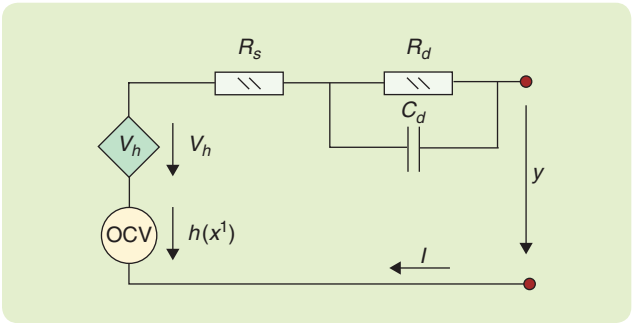

FIGURE 3 An equivalent circuit model corresponding to battery model (3) consists of an RC circuit (R_d, C_d), a series resistor R_s, a hysteresis voltage source V_h, and a voltage source [open circuit voltage (OCV)]. Both the hysteresis voltage and the OCV are state-of-charge (SoC) dependent. The OCV is parameterized by a static function $h(x^1)$, where x^1 is the SoC. Here, $I > 0$ for discharge, and $I < 0$ for charge.

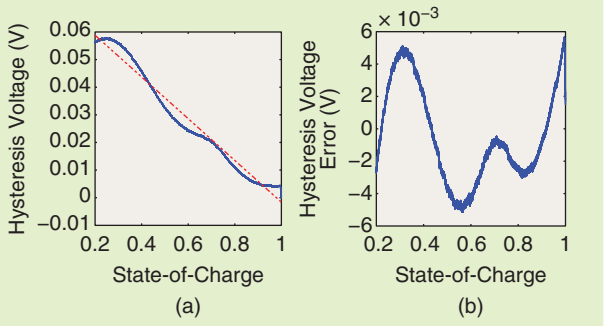

FIGURE 5 The hysteresis voltage, its prediction, and the approximation error. (a) Blue solid line: the true hysteresis voltage V_{hs} (the difference between the charge curve and the average curve); red dashed line: $\hat{V}_{hs}$ predicted by $(1-x^1)s$ with $s = 0.0755$. (b) The prediction error $V_{hs} - \hat{V}_{hs}$.

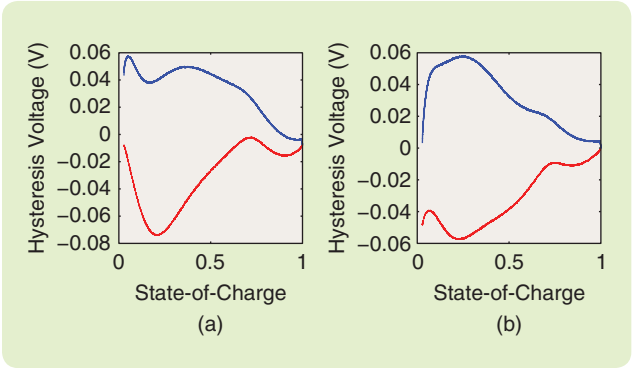

FIGURE 4 The hysteresis voltage V_{hs} as a function of the state-of-charge. Blue line: the difference between the charge curve and the average curve predicted by different parameterizations of $h(x^1)$; red line: the difference between the discharge curve and the average curve predicted by different parameterizations of $h(x^1)$. (a) V_{hs} with parameterization #1: $h(x^1) = a_0 \log(x^1 + a_1) + a_2$. (b) V_{hs} with parameterization #2: $h(x^1) = a_0 \exp(x^1) + a_1 + a_2 x^1 + a_3 (x^1)^2$.

The following notation will be adopted for a vector ζ. Its ith element is denoted by ζ^i. At the kth time step, the ith element is represented by ζ_k^i, and the jth power of ζ_k^i is denoted as $(\zeta_k^i)^j$. $\mathbf{I}_n$ is the $n \times n$ identity matrix. Given a smooth function $h(\zeta)$ and a smooth vector field $f(\zeta)$, the function $L_f h(\zeta) = (\partial h(\zeta)/\partial \zeta) f(\zeta)$ is the Lie derivative of $h(\zeta)$ along $f(\zeta)$, and repeated Lie derivatives $L_f^k h(\zeta) = L_f(L_f^{k-1} h(\zeta))$, $k \geq 1$ with $L_f^0 h(\zeta) = h(\zeta)$.

Offline Model Calibration

Battery model (3) must be calibrated prior to SoC estimation due to the presence of $V_{hs}(x^1)$, $h(x^1)$, and unknown parameters. Calibration of α can be achieved by depleting and then fully charging the battery with small currents. Impedance parameters R_d, C_d, and R_s can be calibrated by: 1) injecting a zero-mean current signal into the battery and collecting the input and output data, 2) linearizing the model (3) around a certain equilibrium $x_e = [x_*^1, 0, 0]^\top$ to obtain a linear time-invariant (LTI) model with linear parameterizations, and 3) following standard procedures to identify parameters [7], [15], [16]. While offline adaptation is straightforward to understand and execute, online adaptation of all parameters is usually preferred. This is particularly true for α because its offline calibration can be rather time consuming and even unrealistic for some practical applications. The same observation extends to the other parameters because they vary with the current, SoC, and temperature.

Specifically, when small constant charge and discharge currents are applied to battery model (3), the voltage across the RC circuit and hysteresis dynamics will both reach equilibria. According to (3), these equilibria can be described as odd functions of the current. Therefore, the true SoC-OCV data can be derived as the average of the charge and discharge SoC-OCV curves.

The next step is to parameterize the functions $h(x^1)$ and $V_{hs}(x^1)$, which relies on a battery's energy-storage dynamics and has been studied by many researchers. As an example, [7] proposes $h(x^1) = a_0 \exp(a_1 x^1) + a_2 + a_3 x^1 + a_4 (x^1)^2 + a_5 (x^1)^3$, where a_j for $0 \leq j \leq 5$ are unknown parameters; in [17], $h(x^1)$ is parameterized by $a_0 \log(x^1 + a_1) + a_2$; whereas [6] takes the Nernst parameterization $h(x^1) = a_0 + a_1 \log(x^1) + a_2 \log(1 - x^1)$. The parameterization of $h(x^1)$ should be determined in a way such that it can predict the true SoC-OCV curve and give rise to a simple expression of the hysteresis voltage $V_{hs}(x^1)$. Ideally, the equilibrium of $V_{hs}(x^1)$ can be represented as a constant so as to allow for a decoupling from x^1 [6]. However, this is not the case for the battery used in the experiment according to the SoC-$V_{hs}(x^1)$ plot shown in Figure 2. Figures 4 and 5 illustrate how to choose the parameterization of $h(x^1)$. As shown in Figure 4, with a fixed x^1 and parameterization #1, $V_{hs}(x^1)$ is not an odd function of I. With parameterization #1, it necessitates two individual functions of $V_{hs}(x^1)$ for the charge and discharge processes. On the other hand, with parameterization #2,

$V_{hs}(x^1)$ is virtually an odd function of I and thus can be represented by one simple function, $V_{hs}(x^1) = s(1-x^1)$, for both charge and discharge processes. Figure 5 verifies that the $\hat{V}_{hs}(x^1)$, if parameterized by $s(1-x^1)$ with $s = 0.0755$, fits the measured data with high precision.

STATE-OF-CHARGE ESTIMATION IN BATTERIES

A BMS enables the safe and efficient use of batteries only when it maintains an accurate estimate of the battery state and parameters including the SoC and SoH. Given the nonlinear battery model and measurements, the SoC and SoH estimation problems can be formulated as nonlinear state and parameter estimation, respectively. The rest of this article will focus on the SoC estimation because state and parameter estimation are mingled and can be addressed through similar techniques [15], [18]. As such, a focus on the SoC estimation can still put SoH estimation into perspective, without compromising the value and contribution of this article.

In this section, both nonadaptive and adaptive SoC estimation problems are examined through a thorough observability and sensitivity analysis. Baseline and new EKF-based SoC estimators are provided and validated using both simulation and experimental data. Synthetic data for simulation are generated from battery model (3) with parameters: $C_0 = 4.9302$ Ah, $R_d = 3\times10^{-3}\Omega$, $C_d = 9\times10^{3}$F, $\gamma = 2.47\times10^{-3}$, $s = 0.0755$, and $R_s = 5\times10^{-3}\Omega$. Experimental data are collected from a 18650-type Li^+ battery cell run on a battery tester at the Advanced Technology R&D Center, Mitsubishi Electric Corporation. The battery cell has a nominal capacity of 4.9302 Ah. The sampling period is $T_s = 1$ s. During the experiment, the ambient temperature in the chamber was maintained at 25.8 ºC. Throughout this section, the default units for voltage and current are V and A, respectively. The battery capacity has units of ampere-hour (Ah). While the performance of estimators can be assessed on multiple metrics, including the root-mean-square error and the ∞-norm of the estimation-error signal, it is known that all norms are equivalent in a certain sense, so the ∞-norm of the SoC estimation error is adopted as the single evaluation metric here for the sake of simplicity.

Nonadaptive State-of-Charge Estimation

Dynamic model-based nonadaptive SoC estimation aims to reconstruct the SoC without parameter adaptation, based on battery model (3) and the current and voltage measurements. Observability analysis of battery model (3) establishes that 1) battery model (3) is not uniformly observable, and 2) with a constant control, battery model (3) is observable almost over the entire range of the SoC. Subsequently, the EKF is applied to solve the nonadaptive SoC estimation problem. Validation using the synthetic and experimental data reveals that the EKF estimator performs well with exact model knowledge but fails to provide accurate estimates in the presence of model-plant mismatch.

Uniform Observability Analysis

Uniform observability is of great importance as a prerequisite for applying diverse nonlinear observer design tools [19], [20]. It is also often a critical condition to establish the convergence of estimation-error dynamics. See "Observability for Nonlinear Systems" for details on uniform observability for nonlinear single-input, single-output (SISO) affine control systems. The state equation of battery model (3) is of the form

$$\dot{x} = f(x) + g(x, \operatorname{sign}(I))I,$$

where $x = [x^1, x^2, x^3]^\top$, $f(x) = [0, -x^2/\tau_d, 0]^\top$ is a smooth vector field with $\tau_d = R_d C_d$, and $g(x, \operatorname{sign}(I)) = [-\alpha, 1/C_d, -\gamma[(1-x^1)s + \operatorname{sign}(I)x^3]]^\top$ is a nonsmooth vector field. With $I = 0$, battery model (3) reduces to the uncontrolled form

$$\begin{aligned} \dot{x} &= f(x), \\ y &= h(x^1) - x^2 + x^3. \end{aligned} \tag{4}$$

A requirement for (3) to be uniformly observable is the observability of the uncontrolled model (4). For (4), the observable coordinates $\phi(x) = [y, L_f y, L_f^2 y]^\top$ are expressed by

$$\begin{aligned} y &= h(x^1) - x^2 + x^3, \\ L_f y &= x^2/\tau_d, \\ L_f^2 y &= -x^2/\tau_d^2. \end{aligned}$$

The Jacobian of the observable coordinates, also referred to as the observability matrix $Q_o(x)$, is singular. The uncontrolled model (4) is not state observable, and thus battery model (3) is not uniformly observable.

An interpretation of the unobservable space can be obtained by considering the LTI system

$$\begin{aligned} \dot{\tilde{x}} &= \begin{bmatrix} 0 & 0 & 0 \\ 0 & -1/\tau_d & 0 \\ 0 & 0 & 0 \end{bmatrix} \tilde{x}, \\ \tilde{y} &= [c_1 \;\; -1 \;\; 1]\tilde{x}, \end{aligned} \tag{5}$$

where $\tilde{x} = x - x_e$, $x_e = [x_*^1, 0, 0]^\top$ with $x_*^1 \in (0,1)$, and $c_1 = \partial h(x^1)/\partial x^1|_{x_*^1}$. System (5) is derived from the linearization of the uncontrolled model (4) around x_e. For an n-dimensional LTI system

$$\begin{aligned} \dot{\zeta} &= A_\zeta \zeta + B_\zeta u, \\ y &= C_\zeta \zeta, \end{aligned} \tag{6}$$

where $\zeta \in \mathbb{R}^n$, state observability can be examined by verifying the rank condition $\operatorname{rank}([\lambda \mathrm{I}_n - A_\zeta^\top, C_\zeta^\top]^\top) = n$ for all eigenvalues λ of A_ζ. Regarding system (5), the rank condition is violated for the eigenvalue $\lambda = 0$. Hence, the unobservable space constitutes an eigenvector corresponding to the eigenvalue $\lambda = 0$.

The observable subspace of the uncontrolled model (4) can also be established. According to [21, Def. 3.29], the observable space is the linear space (over $\mathbb{R}$) of functions $h(x^1) - x^2 + x^3$ and x^2. Similarly, based on [21, Prop. 3.34], the unobservable submanifold is derived

Observability for Nonlinear Systems

Observability is a fundamental system property that concerns whether the system state can be reconstructed from measurements. Its precise characterization relies on state indistinguishablility, which is defined as follows.

Definition S1 (State Indistinguishablility) [S60]
Consider a nonlinear control system

$$\begin{aligned} \dot{\zeta} &= f(\zeta, u), \\ y &= h(\zeta), \end{aligned} \tag{S7}$$

where $\zeta \in \mathbb{R}^n$ is the system state, $u \in \mathbb{R}^m$ the control input, $y \in \mathbb{R}^p$ the output, and f and h are smooth. Two states ζ and $\bar{\zeta}$ are indistinguishable if, for every input $u \in [0, T]$, the system outputs corresponding to two pairs (ζ, u) and $(\bar{\zeta}, u)$ are exactly the same.

A system (S7) is observable if it does not have indistinguishable states. Regarding a single output uncontrolled system, the observability verification is reduced to performing a simple algebraic test, which induces the following observability definition.

Definition S2 (Observability) [S61]
The system

$$\begin{aligned} \dot{\zeta} &= f(\zeta), \quad \zeta \in \mathbb{R}^n, \\ y &= h(\zeta), \quad y \in \mathbb{R}, \end{aligned} \tag{S8}$$

is said to be locally observable in U_0, a neighborhood of the origin, if

$$\operatorname{rank}\{\mathrm{d}h(\zeta), \ldots, \mathrm{d}(L_f^{n-1}h(\zeta))\} = n, \quad \zeta \in U_0. \tag{S9}$$

If (S9) holds for every $\zeta \in \mathbb{R}^n$, then the system is observable.

For a nonlinear control system (S7), observability does not imply that every input distinguishes arbitrary system states, and thus is input dependent. The input-dependent observability is mathematically rigorous but provides little guidance in observer synthesis. Of practical importance is determining whether the system is observable for a given control input [22] or whether the observability is input independent [S61]. Given a control input, the verification of observability for system (S7) is straightforward following Definition S2. The input-independent observability, named after uniform observability, is important and interesting because it enables observer designs for bilinear systems [S62], affine control systems [S61], and nonaffine control systems [22].

Definition S3 (Uniform Observability) [S61, Def. 2]
A SISO controlled nonlinear system

$$\begin{aligned} \dot{\zeta} &= f(\zeta) + g(\zeta)u, x \in \mathbb{R}^n, \\ y &= h(\zeta), \end{aligned} \tag{S10}$$

is uniformly observable if system (S8) is observable, and if system (S10) is observable for any input, that is, on any finite time interval $[0, T]$, for any measurable bounded input $u(t)$ defined on $[0, T]$, the initial state is uniquely determined on the basis of the output $y(t)$ and the input $u(t)$.

Verifying the uniform observability of a generic system is not easy except for certain special cases. For instance, [S61] and [S63] establish necessary and sufficient conditions to guarantee that system (S7) with affine control inputs is uniformly observable.

REFERENCES

[S60] R. Hermann and A. J. Krener, "Nonlinear controllability and observability," *IEEE Trans. Automat. Control*, vol. AC-22, no. 5, pp. 728–740, Oct. 1977.

[S61] J. P. Gauthier, H. Hammouri, and S. Othman, "A simple observer for nonlinear systems–applications to bioreactors," *IEEE Trans. Automat. Control*, vol. 37, no. 6, pp. 875–880, 1992.

[S62] D. Williamson, "Observation of bilinear systems with application to biological control," *Automatica*, vol. 13, no. 3, pp. 243–254, 1977.

[S63] J. P. Gauthier and I. Kupka, *Deterministic Observation Theory and Applications*. Cambridge, U.K.: Cambridge Univ. Press, 2001.

as $S_0 = \{x \,|\, h(x^1) - x^2 + x^3 = 0, x^2 = 0\}$. Physical interpretation of the unobservable submanifold is that with $I = 0$, both the hysteresis voltage x^3 and the OCV stay constant, but only their sum can be inferred from the output. Hence, x^1 and x^3 are indistinguishable.

Observability Analysis: Constant Control Case

In demonstrating the basic procedure for observability analysis, the above shows that zero control input will render battery model (3) unobservable. However, this does not imply the infeasibility of SoC estimation. Since SoC estimation is meaningful during battery operation, it is more relevant to investigate whether battery model (3) is observable when practical control inputs exist. Similar problems have been studied for general nonaffine control systems [22]. Observability analysis can be performed when battery model (3) is subject to a specific form of control inputs.

For illustration purposes, the observability analysis is performed when battery model (3) is subject to constant control inputs. Without loss of generality, assume $I = I_0 > 0$ with I_0 constant. Battery model (3) is rewritten as $\dot{x} = f(x), y = h(x^1) - x^2 + x^3 - R_s I_0$ with $f(x) = [-\alpha I_0, -x^2/\tau_d + I_0/C_d, -\gamma I_0[(1 - x^1)s + x^3]]^\top$. The observable coordinates are

$$\begin{aligned} y &= h(x^1) - x^2 + x^3 - R_s I_0, \\ L_f y &= -\alpha I_0 \frac{\partial h(x^1)}{\partial x^1} + \frac{x^2}{\tau_d} - \frac{I_0}{C_d} - \gamma[s(1 - x^1) + x^3], \\ L_f^2 y &= \alpha I_0 \left[\alpha I_0 \frac{\partial^2 h(x^1)}{\partial (x^1)^2} - \gamma s\right] - \frac{x^2}{\tau_d^2} + \frac{I_0}{\tau_d C_d} + \gamma^2[s(1 - x^1) + x^3], \end{aligned}$$

and the observability matrix is given by

$$Q_o(x, I_0) = \begin{bmatrix} \dfrac{\partial h(x^1)}{\partial x^1} & -1 & 1 \\ \gamma s - \dfrac{\partial^2 h(x^1)}{\partial (x^1)^2}\alpha I_0 & \dfrac{1}{\tau_d} & -\gamma \\ \alpha^2 I_0^2 \dfrac{\partial^3 h(x^1)}{\partial (x^1)^3} - \gamma^2 s & -\dfrac{1}{\tau_d^2} & \gamma^2 \end{bmatrix}.$$

The determinant of the observability matrix is $\det(Q_o) = 1/\tau_d^2 \rho(x^1)(\gamma\tau_d - 1)$, where

$$\rho(x^1) = \frac{\partial^3 h(x^1)}{\partial (x^1)^3}\alpha^2 \tau_d I_0^2 - \alpha I_0 \frac{\partial^2 h(x^1)}{\partial (x^1)^2}(\gamma\tau_d + 1) + \frac{\partial h(x^1)}{\partial x^1}\gamma + \gamma s.$$

The observability matrix is singular only when one of the following conditions holds:

- $\gamma\tau_d = 1$, which holds only if the RC circuit and the hysteresis voltage dynamics have exactly the same time constant.
- $\rho(x^1) = 0$, which imposes conditions on the function $h(x^1)$. With $(\partial^3 h(x^1)/\partial (x^1)^3) > 0, (\partial^2 h(x^1)/\partial (x^1)^2) < 0$, and $(\partial h(x^1)/\partial (x^1)) > 0$, for almost all $x^1 \in [0,1]$, as shown in Figure 6, it follows that $\rho(x^1) > 0$.

Battery model (3) with nonzero constant control inputs is therefore observable for almost all $x^1 \in [0,1]$.

A nonsingular observability matrix, however, is not enough to guarantee accurate state estimation because the state-estimation performance can be compromised by the existence of weakly observable modes [23], [24]. A linear system is weakly observable if the observability matrix is ill-conditioned. Similar criteria have been used for nonlinear systems [25]. The observability matrix of a nonlinear system often depends on the control inputs. A common practice is to check the observability matrix for a given control input. As an example, the observability matrix of battery model (3) is checked for a constant current input $I = 2$C-rates, with the condition number plotted in Figure 7. The observability matrix has condition number on the order of 10^4. Despite a possible issue for a high-dimensional matrix, the condition number of around 10^4 is not a problem for a 3×3 matrix [26]. The nonadaptive SoC estimation problem is therefore considered well posed.

Observability analysis of battery model (3) can be alternatively conducted in nonlinear switched-system setting, since (3) can be reformulated as a switched system with $g(x, \text{sign}(I)) = [-\alpha, 1/C_d, -\gamma[(1-x^1)s + x^3]]^\top$, for $I \geq 0$, or $g(x, \text{sign}(I)) = [-\alpha, 1/C_d, -\gamma[(1-x^1)s - x^3]]^\top$ otherwise (see [27] for details).

Applicability of the Extended Kalman Filter

The observability analysis above shows that battery model (3) is not transformable to special structures due to the deficiency of uniform observability and thus defies many commonly used nonlinear observer designs, such as normal-

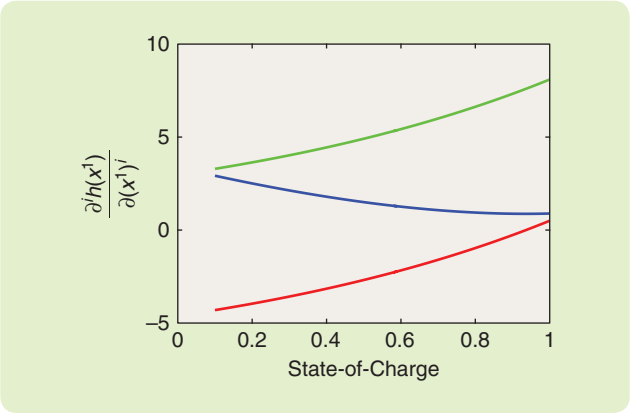

FIGURE 6 Derivatives of the open circuit voltage with respect to the state-of-charge. Blue line: $(\partial h(x^1)/\partial x^1)$; red line: $(\partial^2 h(x^1)/\partial (x^1)^2)$; and green line: $(\partial^3 h(x^1)/\partial (x^1)^3)$.

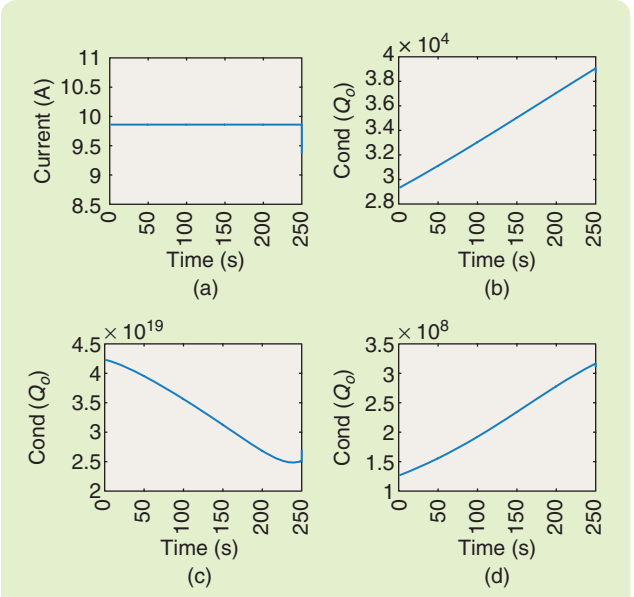

FIGURE 7 Condition numbers of the observability matrix Q_o when different battery models are subject to the constant current. (a) The constant current profile, (b) the third-order battery model (3), (c) the eighth-order augmented battery model, and (d) the fourth-order augmented battery model.

form-based observer designs [19], [22], [28]–[36]. On the other hand, nonlinear stochastic-estimation techniques do not impose such restrictions on the system structure. The incentive to explore SoC estimation in the stochastic framework is further strengthened by the practical necessity to accommodate measurement and process noises. Thus, in this regard, nonlinear stochastic estimators such as the EKF, the unscented KF [37], [38], the ensemble KF [39]–[41], the particle filter [42], and the moving-horizon estimator [43] are preferable because they can deal with noise and quantify uncertainties and confidence intervals of the estimates. Compared with the particle filter and the moving-horizon

estimator [43], the EKF is attractive because it is relatively easy to design and implement and has only moderate computational expense for low-order systems. However, the EKF suffers from several shortcomings, such as performance degradation due to linearization-induced errors or non-Gaussian noises, lack of stability results, and large computational costs for high-dimensional systems. The advantages still outweigh the disadvantages for low-dimensional stochastic systems as many real-world applications are. Therefore, the EKF is still an appealing tool for industrial practitioners. As such, the EKF is promising as a solution for the nonadaptive SoC estimation problem. A consideration of the noise and linearization error for SoC estimation below will corroborate this point.

Noise in sensors and actuators of the BMS mainly come from quantization errors, constant offsets, and noise due to power electronics. The constant offsets in sensors and actuators can be readily dealt with by introducing constant bias parameters in the estimator [23], [44]. Noise from power electronics is typically at much higher frequencies than the sampling frequency or the bandwidth of the battery dynamics and thus is negligible. There has been much research toward analyzing the stochastic properties of a quantization error and mitigating its adverse effects on control systems. For instance, [45] establishes necessary and sufficient conditions to ensure that the quantization error is white and additive. Reference [46] establishes that uniform quantization often leads to additive quantization errors with white spectrum. In [47], the effects of different quantization schemes on KF-based state estimation for LTI systems are analyzed, and it is demonstrated that certain quantization schemes render the output error $y-\hat{y}$ an asymptotic Gaussian process, validating the KF-based state estimation. Thus, it is appropriate to assume that the quantizers have been designed to produce white and additive quantization errors. Last but not least, the detrimental effects of the linearization-induced error on the EKF-based SoC estimation are insignificant because:

- Battery model (3) does not possess strong nonlinearity. Specifically, the state equation is linear in the state; as shown in Figure 6, the nonlinearity in the output equation has a gradient bounded by [0.75,3];
- The model-plant mismatch due to linearizing the output equation can be effectively alleviated by setting the initial SoC of the EKF estimator close to the true value. This is possible because the output y is dominated by the OCV and thus can be used to generate a good initial guess of the SoC.

Extended Kalman Filter-Based State-of-Charge Estimation

To facilitate the EKF-based nonadaptive SoC estimation, battery model (3) is discretized to give the discrete-time model

$$\begin{aligned} x_{k+1} &= A_k(\theta,u_k)\,x_k + B_k(\theta,u_k)\,u_k + w_k^x,\\ y_k &= h(x_k^1) - x_k^2 + x_k^3 - \theta^5 I^k + v_k, \end{aligned} \tag{7}$$

where $\theta=[\theta^1,\ldots,\theta^5]^\top$, k is the time index, $u_k=[I_k;1]^\top$, $w_k^x=[w_k^1,\ldots,w_k^3]^\top$ includes the process noises, and v_k is the measurement noise. The noise covariances are $W_k^x = E[w_k^x(w_k^x)^\top] = \text{diag}\{W_k^1,\ldots,W_k^3\}$ and $V_k = E[(v_k)^2]$. Matrices in (7) are

$$A_k(\theta)=\begin{bmatrix} 1 & 0 & 0\\ 0 & \theta^2 & 0\\ (1-(\theta^4)^{|I_k|})\,\text{sign}(I_k)\,s & 0 & (\theta^4)^{|I_k|}\end{bmatrix}$$

$$\text{and}\quad B_k(\theta)=\begin{bmatrix} -\theta^1 & 0\\ \theta^3 & 0\\ 0 & ((\theta^4)^{|I_k|}-1)\,\text{sign}(I_k)\,s\end{bmatrix},$$

where $\theta^1=\alpha T_s$, $\theta^2=\exp(-T_s/\tau_d)$, $\theta^3=R_d(1-\theta^2)$, $\theta^4=\exp(-\gamma T_s)$, $\theta^5=R_s$, $s=0.0755$, and $T_s=1$ s is the sampling period. For ease of presentation, x_k^1 is treated as a constant during the discretization of the hysteresis-voltage dynamics.

The sampling period is determined by battery dynamics, the sensor resolution, and computation resources. Given that the time constant of battery dynamics is typically longer than 10 s [6], [7], [13], [14], the sampling period can be a few seconds. On the other hand, the sampling period should be long enough so that the data-acquisition hardware in the BMS can produce accurate readings. Accuracy is primarily constrained by the sensor resolution, the impact of which can be exemplified by the voltage sensor. Based on the specification of the battery terminal voltage, the voltage sensor range can be selected as [0,5] V. With a 12-b A/D converter, the resolution of the voltage sensor is $5/2^{12}=0.0012$ V. As pointed out in [48], typical electric vehicles and hybrid electric vehicles are ideally discharged at 1–3 C-rates. Assume that the battery is charged at 3 C-rates. The SoC increases at a rate of 0.084% V/s. Considering the gradient plot in Figure 6, the terminal voltage increases at the rate ranging [0.00063, 0.00252] V/s. The changes of the terminal voltage within a sampling period $T_s=1$ s can be barely detected by the voltage sensor. Hence, a sampling period shorter than 1 s will be unnecessary.

Given the discretized model (7), the EKF design for the full-state estimation follows the steps in "Extended Kalman Filter" and thus is omitted. The EKF-based nonadaptive SoC estimator is first validated by synthetic data, which are generated by exciting the discretized model (7) with two current profiles: pulses and an urban dynamometer driving schedule (UDDS). The initial conditions (ICs) of the battery model and the EKF estimator are taken as $x_0=[0.95,0.1,10^{-3}]^\top$ and $\hat{x}_0=x_0/2$, respectively. The tuning parameters of the EKF are $Q^x=10^{-4}\mathbf{I}_3, R=10^{-4}$, and $P_0=0.5\mathbf{I}_3$. The EKF estimator is fairly robust to changes in Q and R, and the tuning is straightforward. Simulation results for both the pulse and the UDDS current profiles are shown in Figures 8 and 9. When both the discretized model (7) and the EKF estimator use the same values of model parameters, the SoC estimates converge to the true states. However, when the parameter values

are incorrect by 20%, the EKF estimator could not give convergent SoC estimates.

The EKF-based nonadaptive SoC estimator is further validated by experimental data, with results shown in Figure 10, which reveals that the SoC estimation is unsatisfactory. This is because the model parameter values used in the EKF estimator may differ from the truth. Since no parameter adaption is used here, the plant-model mismatch remains throughout the entire estimation process, which impacts the estimation performance.

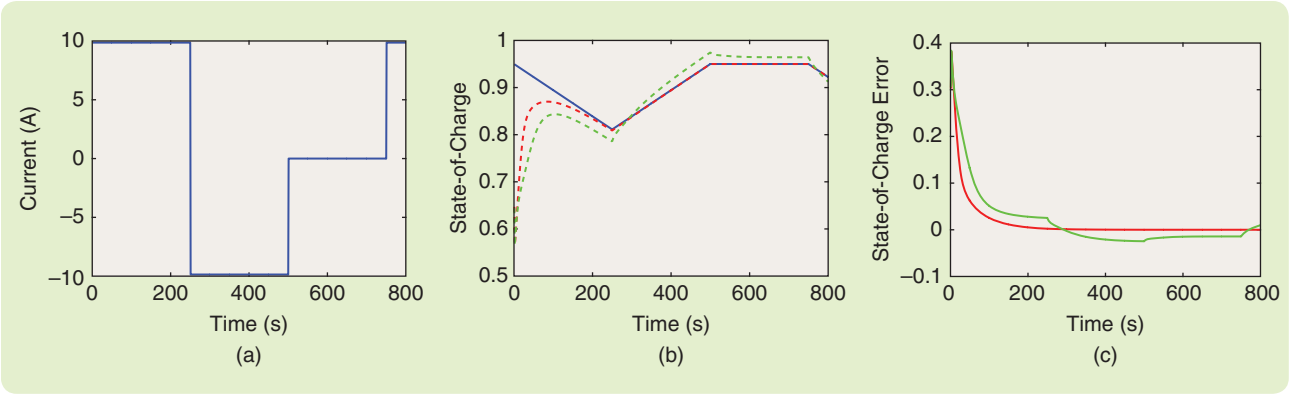

FIGURE 8 A validation of extended Kalman filter-based nonadaptive state-of-charge (SoC) estimator using synthetic data pulse-current case. (a) Pulse-current profile. (b) Blue solid line: true SoC; red dashed line: SoC estimated by using true values of model parameters; green dashed line: SoC estimated where model parameters are 20% off from true values. (c) Red dashed line: SoC estimation error with true values of model parameters; green dashed line: SoC estimation error where model parameters are 20% off from true values.

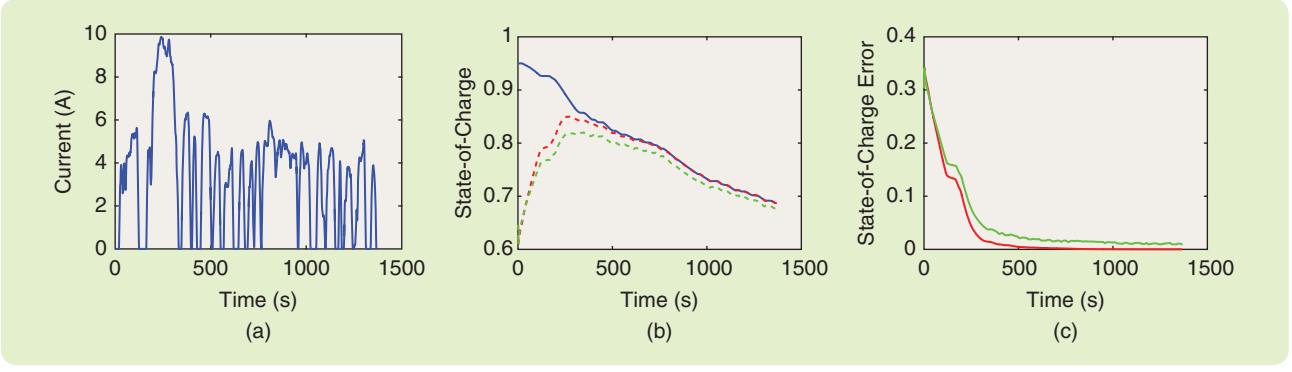

FIGURE 9 A validation of the extended Kalman filter-based nonadaptive state-of-charge (SoC) estimator using synthetic data, urban dynamometer driving schedule (UDDS) current case. (a) UDDS current profile. (b) Blue solid line: true SoC; red dashed line: SoC estimated by using true values of model parameters; green dashed line: SoC estimated where model parameters are 20% off from true values. (c) Red dashed line: SoC estimation error with true values of model parameters; green dashed line: SoC estimation error where model parameters are 20% off from true values.

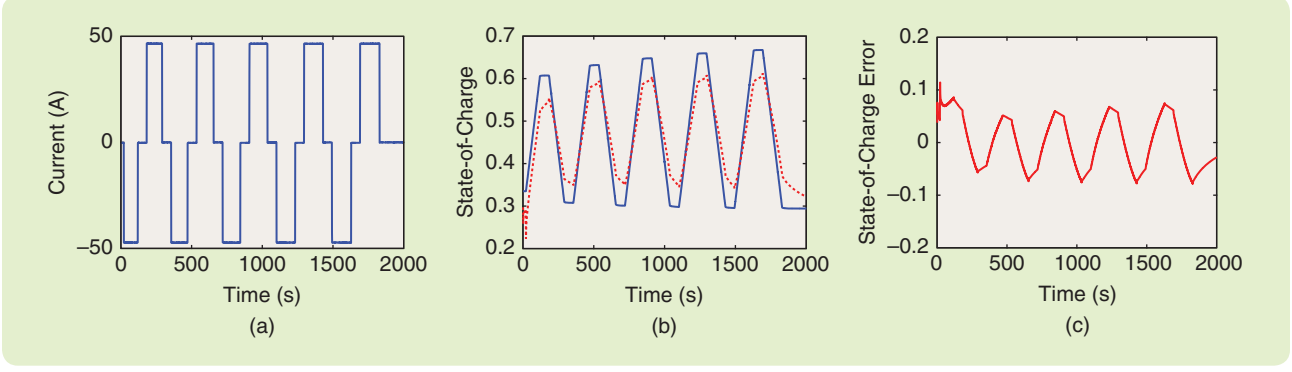

FIGURE 10 A validation of the extended Kalman filter (EKF)-based nonadaptive state-of-charge (SoC) estimator by experimental data. (a) The current profile in the experiment. (b) Blue solid line: true SoC from the Coulomb counting; red dashed line: estimated by the EKF. (c) The SoC estimation error.

Two-Stage Extended Kalman Filter

The two-stage EKF aims to reduce the computational cost of the joint EKF while maintaining comparable performance. The basic idea is that the computational complexity can be reduced by decomposing the high-order joint EKF into multiple low-order filters. This notion has been employed to develop a two-stage KF in [S64], where the KF is decomposed into two parallel, but coupled, reduced-order filters. Due to its ad hoc decomposition, the two-stage KF is not exactly equivalent to the KF and therefore potentially suboptimal. An optimal two-stage KF (OTSKF) is developed and mathematically equivalent to the KF [S65]. The OTSKF applies linear state transformations to diagonalize the estimation-error covariance matrices and achieves a complete decoupling of two reduced-order filters. The state-transformation-based diagonalization and decoupling stimulated extensions of the OTSKF, such as the OTSKF for time-varying and disturbance-driven systems [S66], [S67], the multistage KF [S68], the optimal two-stage EKF (OTSEKF) for nonlinear systems [S69], and the optimal two-stage EKF for linear parameter-varying systems [S70]. It is noteworthy that the OTSEKF involves nonlinear state transformations and thus incurs a relatively high computational burden.

Consider a nonlinear discrete-time system

$$\begin{aligned} x_{k+1} &= f(x_k,\theta_k,u_k)+w_k^x,\\ y_k &= h(x_k,\theta_k,u_k)+v_k,\\ \theta_{k+1} &= g(\theta_k)+w_k^\theta, \end{aligned} \tag{S11}$$

where $x_k\in\mathbb{R}^{n_x}$ is the system state, $\theta_k\in\mathbb{R}^{n_\theta}$ the parameter, $y_k\in\mathbb{R}^{n_y}$ the output, $u_k\in\mathbb{R}^{n_u}$ the input, $f\colon\mathbb{R}^{n_x}\times\mathbb{R}^{n_\theta}\times\mathbb{R}^{n_u}\to\mathbb{R}^{n_x}$, $h\colon\mathbb{R}^{n_x}\times\mathbb{R}^{n_\theta}\times\mathbb{R}^{n_u}\to\mathbb{R}^{n_y}$, and $g\colon\mathbb{R}^{n_\theta}\to\mathbb{R}^{n_\theta}$. The sequences $\{w_k^x\}$, $\{w_k^\theta\}$, and $\{v_k\}$ are zero-mean Gaussian random processes with covariance matrices of Q_k^x, Q_k^θ, and R_k, respectively, and $\{w_k^x\},\{w_k^\theta\}$, and $\{v_k\}$ are independent of each other. System (S11) is also referred as the augmented system with the augmented state $x_k^a=[x_k^\top,\theta_k^\top]^\top$. The joint EKF for the augmented system can be designed as described in "Extended Kalman Filter."

Assume that the two-stage EKF has state estimates $\hat{x}_{k|k}^a$ and $\hat{x}_{k|k-1}^a$, covariance matrices $P_{k|k}^a$ and $P_{k|k-1}^a$, and the gain matrix K_k^a. Next, the formula is derived for the two-stage EKF. Different from the OTSEKF, the two-stage EKF adopts linear state transformations $\bar{x}_{k|k-1}^a=T(-U_k)\hat{x}_{k|k-1}^a$ and $\bar{x}_{k|k}^a=T(-V_k)\hat{x}_{k|k}^a$ to block diagonalize covariance matrices $P_{k|k}^a$ and $P_{k|k-1}^a$, respectively. As in [S65], the transformation matrices take the form

$$T(M)=\begin{bmatrix} I^{n_x\times n_x} & M\\ 0 & I^{n_\theta\times n_\theta}\end{bmatrix},$$

where $M\in\mathbb{R}^{n_x\times n_\theta}$ is the argument matrix to be determined. Note that $T^{-1}(M)=T(-M)$. In the transformed state coordinates, $P_{k|k-1}^a, P_{k|k}^a$, and K_k^a are given by

$$\begin{aligned} \bar{P}_{k|k-1}^a &= T(-U_k)P_{k|k-1}^aT(-U_k)^\top,\\ \bar{P}_{k|k}^a &= T(-V_k)P_{k|k}^aT(-V_k)^\top,\\ \bar{K}_k^a &= T(-V_k)K_k^a. \end{aligned}$$

Matrices $\bar{P}_{k|k-1}^a$ and $\bar{P}_{k|k}^a$ become block diagonal, and thus two reduced-order filters are decoupled.

The two-stage EKF estimation for the augmented system can be performed in the new state coordinates. Figure S2 shows the two-stage EKF scheme, which is summarized as follows.

Initialization: Given the ICs $\hat{x}_{0|0}^a=[\hat{x}^\top,\hat{\theta}^\top]^\top$ and $P_{0|0}^a$, the ICs for the two-stage EKF in the transformed coordinates are $\bar{P}_{0|0}^\theta=P_{0|0}^\theta$, $V_0=P_{0|0}^{x\theta}(P_{0|0}^\theta)^{-1}$, $\bar{\theta}_{0|0}=\hat{\theta}_{0|0}$, $\bar{x}_{0|0}=\hat{x}_{0|0}-V_0\bar{\theta}_{0|0}$, and $\bar{P}_{0|0}^x=P_{0|0}^x-V_0P_{0|0}^\theta V_0^\top$. Matrices $P_{0|0}^x$ and $P_{0|0}^\theta$ are the initial error covariance matrices of the state and parameter, respectively, and $P_{0|0}^{x\theta}$ is the initial error cross-covariance matrix between the state and parameter.

State and parameter prediction: By linearization of f and g at $(\hat{x}_{k|k},\hat{\theta}_{k|k},u_k)$, and h at $(\hat{x}_{k+1|k},\hat{\theta}_{k+1|k},u_k)$, compute matrices $A_k=\partial f/\partial x_k$, $B_k^\theta=\partial f/\partial\theta_k$, $B_k^u=\partial f/\partial u_k$, $G_k=\partial g/\partial\theta_k$, $C_k=\partial h/\partial x_k$, $D_k^\theta=\partial h/\partial\theta_k$, $D_k^u=\partial h/\partial u_k$, and

$$\begin{aligned} \bar{x}_{k|k-1} &= f(\bar{x}_{k-1|k-1},\bar{\theta}_{k-1|k-1},u_{k-1})+(A_{k-1}V_{k-1}-U_kG_k)\bar{\theta}_{k-1|k-1},\\ \bar{\theta}_{k|k-1} &= g(\bar{\theta}_{k-1|k-1}),\\ \bar{P}_{k|k-1}^x &= A_{k-1}\bar{P}_{k-1|k-1}^xA_{k-1}^\top+\bar{Q}_k^x,\\ \bar{Q}_k^x &= Q_{k-1}^x-\bar{U}_k(Q_{k-1}^\theta)^\top,\\ U_k &= \bar{U}_k-\bar{U}_kQ_k^\theta(P_{k|k-1}^\theta)^{-1},\\ \bar{U}_k &= (A_{k-1}V_{k-1}+B_{k-1}^\theta)G_{k-1}^{-1},\\ \bar{P}_{k|k-1}^\theta &= G_{k-1}\bar{P}_{k-1|k-1}^\theta G_{k-1}^\top+Q_{k-1}^\theta. \end{aligned}$$

Adaptive State-of-Charge Estimation

As shown above, nonadaptive SoC estimation fails to deliver adequate performance in the experimental validation. This does not come as a surprise because an exact knowledge of the battery parameters is absent, which is often likely to happen in practice. Even worse, the battery parameters can fluctuate with the input current, SoC, or temperature. Adaptive SoC estimation, therefore, is of considerable importance in the real-world battery use, with its capability of updating the parameter values in real time to provide a better model. This section offers a series of EKF-based adaptive SoC estimators. For self-completeness and comparison purposes, a baseline joint EKF estimator is first presented to expose its weaknesses: the relatively high computational cost and tuning efforts. The high

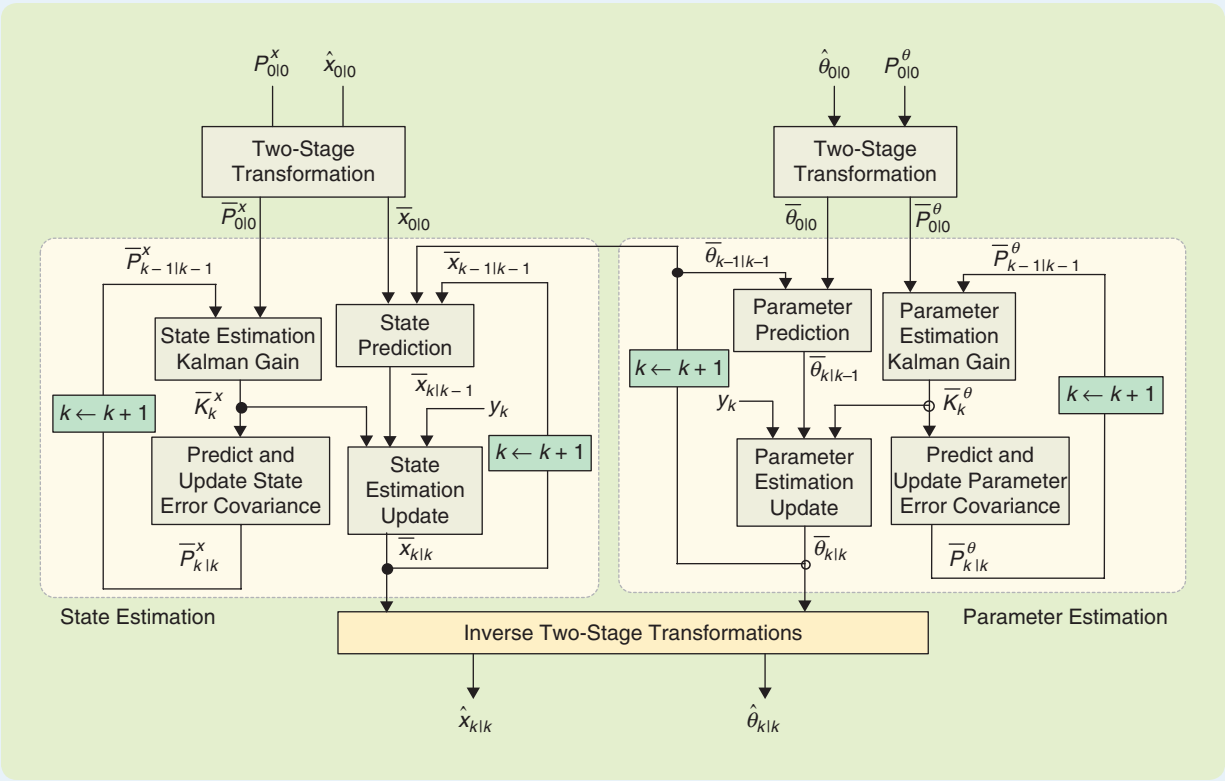

FIGURE S2 A two-stage extended Kalman filter block diagram.

State and parameter update:

$$
\begin{aligned}
\bar{K}^x_k &= \bar{P}^x_{k|k-1} C_k^\top (C_k \bar{P}^x_{k|k-1} C_k^\top + R_k)^{-1},\\
\bar{x}_{k|k} &= \bar{x}_{k|k-1} + \bar{K}^x_k (y_k - h(\bar{x}_{k|k-1}, \bar{\theta}_{k|k-1}, u_k)),\\
\bar{P}^x_{k|k} &= \bar{P}^x_{k|k-1} - \bar{K}^x_k C_k \bar{P}^x_{k|k-1},\\
\bar{\theta}_{k\,|\,k} &= \bar{\theta}_{k\,|\,k-1} + \bar{K}^\theta_k (y_k - h(\bar{x}_{k\,|\,k-1}, \bar{\theta}_k, u_k)) - S_k \bar{\theta}_{k\,|\,k-1},\\
\bar{K}^\theta_k &= \bar{P}^\theta_{k|k-1} S_k^T (C_k \bar{P}^x_{k|k-1} C_k^\top + R_k + S_k^T \bar{P}^\theta_{k|k-1} S_k^T)^{-1},\\
\bar{P}^\theta_{k|k} &= \bar{P}^\theta_{k|k-1} - \bar{K}^\theta_k S_k \bar{P}^\theta_{k|k-1},\\
S_k &= C_k U_k + D^\theta_k,\\
V_k &= U_k - \bar{K}^x_k S_k.
\end{aligned}
$$

The state-estimate $\hat{x}^a$ can be recovered by the inverse two-stage state transformation as $\hat{x}^a_{k|k-1} = T(U_k)\bar{x}^a_{k|k-1}$, $\hat{x}^a_{k|k} = T(V_k)\bar{x}^a_{k|k}$.

REFERENCES

[S64] B. Friedland, "Treatment of bias in recursive filtering," *IEEE Trans. Automat. Control*, vol. 14, no. 4, pp. 359–367, Aug. 1969.

[S65] C.-S. Hsieh and F.-C. Chen, "Optimal solution of the two-stage Kalman estimator," *IEEE Trans. Automat. Control*, vol. 44, no. 1, pp. 194–199, 1999.

[S66] C.-S. Hsieh and F.-C. Chen, "General two-stage Kalman filters," *IEEE Trans. Automat. Control*, vol. 45, no. 4, pp. 819–824, 2000.

[S67] C.-S. Hsieh, "Robust two-stage Kalman filters for systems with unknown inputs," *IEEE Trans. Automat. Control*, vol. 45, no. 12, pp. 2374–2378, 2000.

[S68] F.-C. Chen and C.-S. Hsieh, "Optimal multistage Kalman estimators," *IEEE Trans. Automat. Control*, vol. 45, no. 11, pp. 2182–2188, 2000.

[S69] C.-S. Hsieh, "General two-stage extended Kalman filters," *IEEE Trans. Automat. Control*, vol. 48, no. 2, pp. 289–293, 2003.

[S70] M. Hilairet, F. Auger, and E. Berthelot, "Speed and rotor flux estimation of induction machines using a two-stage extended Kalman filter," *Automatica*, vol. 45, no. 8, pp. 1819–1827, 2009.

computation cost is alleviated leveraging a two-stage EKF described in "Two-Stage Extended Kalman Filter." The tuning difficulty is addressed by sensitivity analysis, which singles out a set of most identifiable parameters to exclude weakly observable modes. Based on the sensitivity analysis, an enhanced adaptive SoC estimator is developed. Finally, simulation and experiments demonstrate the effectiveness of both the enhanced adaptive SoC estimator and the two-stage EKF design.

Joint Extended Kalman Filter Approach

A joint EKF frequently appears as a viable solution for many applications involving state and parameter estimation. A comprehensive description of its application to adaptive SoC estimation is presented in [49]. The joint

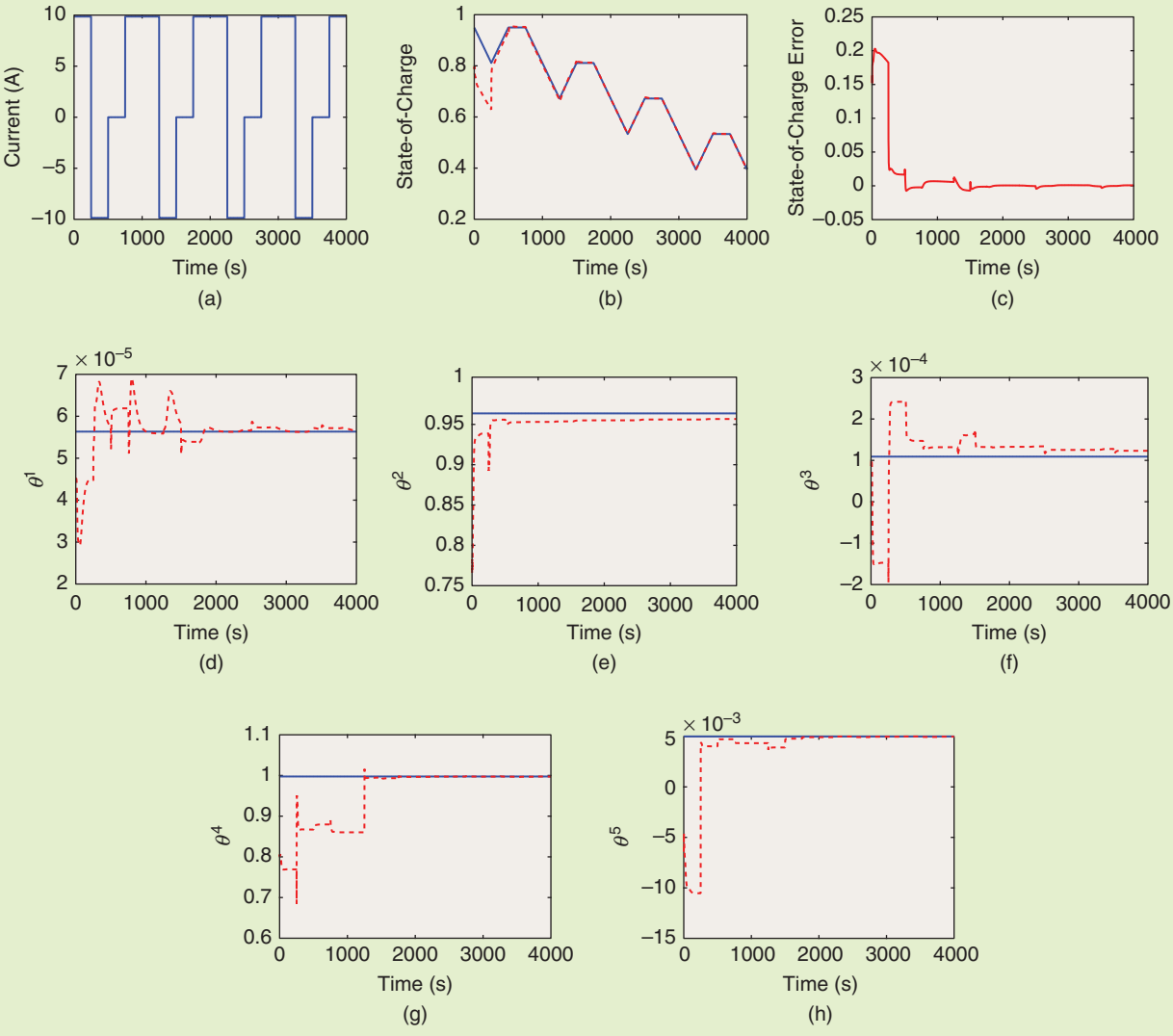

FIGURE 11 A validation of the joint extended Kalman filter (EKF)-based adaptive state-of-charge (SoC) estimator by synthetic data pulse-current case. (a) Current profile. (b) Blue solid line: true SoC; red dashed line: estimated. (c) SoC estimation error. (d) Blue solid line: true θ^1; red dashed line: estimated. (e) Blue solid line: true θ^2; red dashed line: estimated. (f) Blue solid lie: true θ^3; red dashed line: estimated. (g) Blue solid line: true θ^4; red dashed line: estimated. (h) Blue solid line: true θ^5; red dashed line: estimated. Consistent with analysis results, tuning of the joint EKF is difficult to make the estimate of θ^2 and θ^4 converge.

EKF-based adaptive SoC estimator is based on the augmented battery model

$$x_{k+1}^a = \begin{bmatrix} A_k(\theta_k, u_k)x_k + B_k(\theta_k, u_k)u_k \\ \theta_k \end{bmatrix} + \begin{bmatrix} w_k^x \\ w_k^\theta \end{bmatrix},$$
$$y_k = h(x_k^1) - x_k^2 + x_k^3 - \theta_k^5 I_k + v_k, \tag{8}$$

where $x_k^a = [x_k^\top, \theta_k^\top]^\top \in \mathbb{R}^8$ is the augmented state and $w_k^\theta = [w_k^4, \ldots, w_k^8]^\top$ $w_k^\theta = [w_k^4, \ldots, w_k^8]^\top$ with the covariance matrix $W_k^\theta = E[w_k^\theta (w_k^\theta)^\top] = \text{diag}\{W_k^4, \ldots, W_k^8\}$. The augmented battery model (8) is derived by assuming battery parameters are constant, which is arguably valid when battery parameters vary at a temporal scale much larger than the sampling period. Fluctuations of the temperature and SoC are typically slow, and thus their influences on battery parameters can be characterized by the term w_k^θ. The charge rate might change faster than the sampling rate, and the resultant parameter variations cannot be captured by model (8). This limitation, however, can be addressed by considering rate-dependent parameter models as in [7]. It is not theoretically justifiable to assume a diagonal W_k^θ, because the components of w_k^θ are induced by the state and temperature variation and are thus correlated.

Given the augmented model (8), the joint EKF-based adaptive SoC estimator can be readily developed using the process in "Extended Kalman Filter." For the simulation of the joint EKF-based adaptive SoC estimator with the synthetic data, its ICs and tuning parameters are

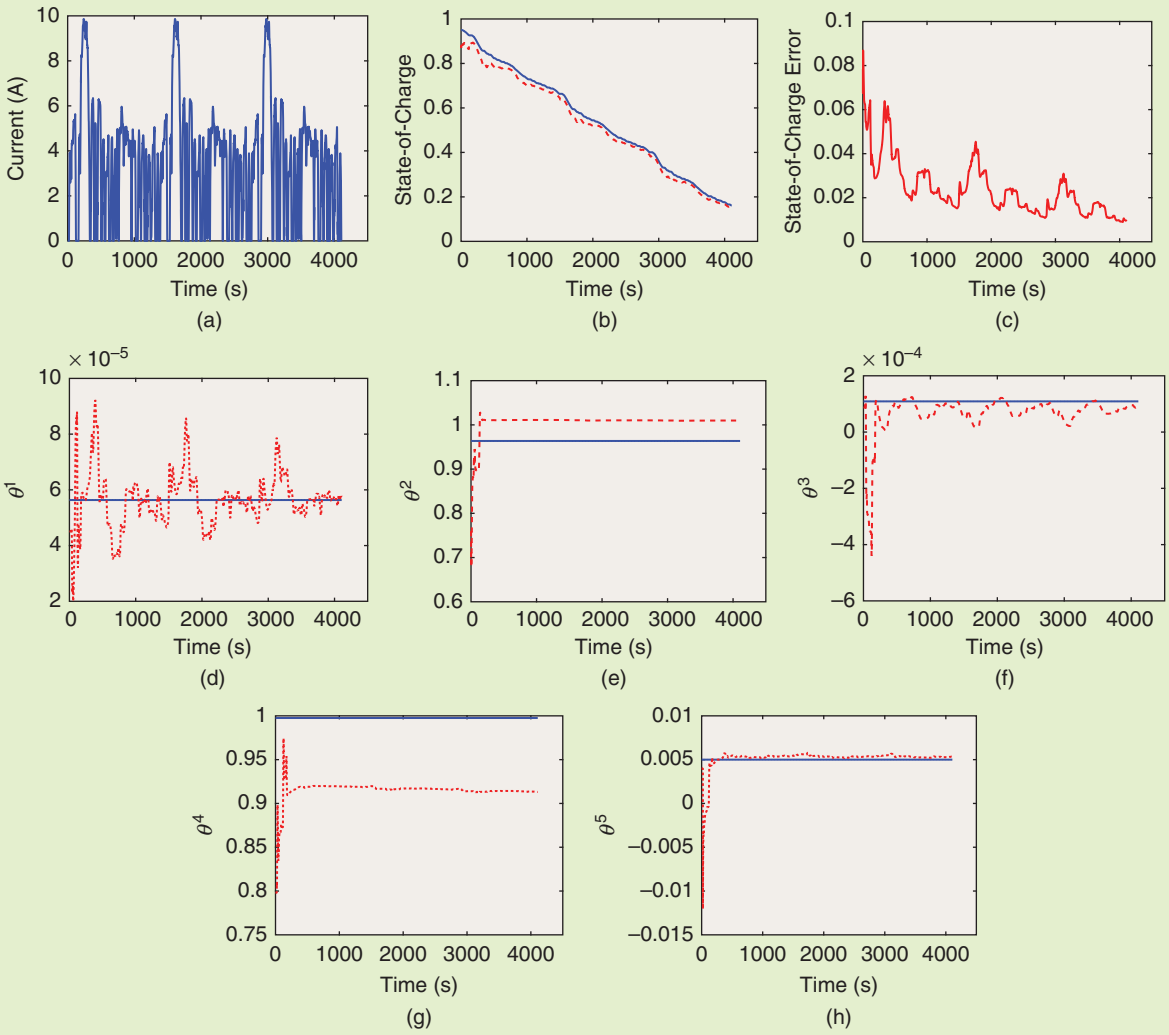

FIGURE 12 A validation of the joint extended Kalman filter (EKF)-based adaptive state-of-charge (SoC) estimator by synthetic data, urban dynamometer driving schedule (UDDS) current case. (a) The UDDS current profile. (b) Blue solid line: true SoC; red dashed line: estimated. (c) SoC estimation error. (d) Blue solid line: true θ^1; red dashed line: estimated. (e) Blue solid line: true θ^2; red dashed line: estimated. (f) Blue solid line: true θ^3; red dashed line: estimated. (g) Blue solid line: true θ^4; red dashed line: estimated. (h) Blue solid line: true θ^5; red dashed line: estimated. Consistent with analysis results, tuning of the joint EKF is difficult to make the estimates of θ^2 and θ^4 converge.

$$\hat{x}_0^a = [0.75x_0^\top, 0.8\theta_0^\top]^\top,$$
$$Q = \text{diag}\{10^{-6}, 10^{-8}, 10^{-8}, 5\times 10^{-11}, 10^{-8}, 10^{-10}, 10^{-4}, 10^{-8}\},$$
$$R = 10^{-4},$$
$$P_0 = \text{diag}\{0.0625, 0.01, 10^{-6}, 10^{-10}, 0.0625, 10^{-7}, 0.0625, 10^{-3}\},$$

where $x_0 = [0.95, 0.1, 10^{-3}]^\top$ is the true state, and $\theta_0 = [6.94\times 10^{-5}, 0.989, 3.31\times 10^{-4}, 0.998, 0.08]^\top$ is the true parameter values, computed according to nominal values of R_s, R_d, C_d, R_s, and C_0. Simulation results are given in Figure 11 for the pulse current and Figure 12 for the UDDS current. Simulation results for both current profiles lead to the following observations:

- Unlike the nonadaptive case, the joint EKF-based adaptive SoC estimator can provide accurate SoC estimation.
- Significant effort is required to tune the Q and P_0 to ensure the convergence of the state and parameter estimation. Parameters θ^2, θ^4 are much more difficult to estimate than other parameters. This is consistent with the sensitivity analysis offered below.
- The adaptive SoC estimator takes longer to converge than the nonadaptive case. This is expected due to the additional parameter identification process.

The joint EKF estimator is also verified by the experimental data, as shown in Figure 13. Both simulation and experimental studies confirm that the adaptive SoC estimation outperforms the nonadaptive case in terms of the estimation accuracy, though it should be noted that tuning the joint EKF for adaptive SoC estimation is more time consuming.

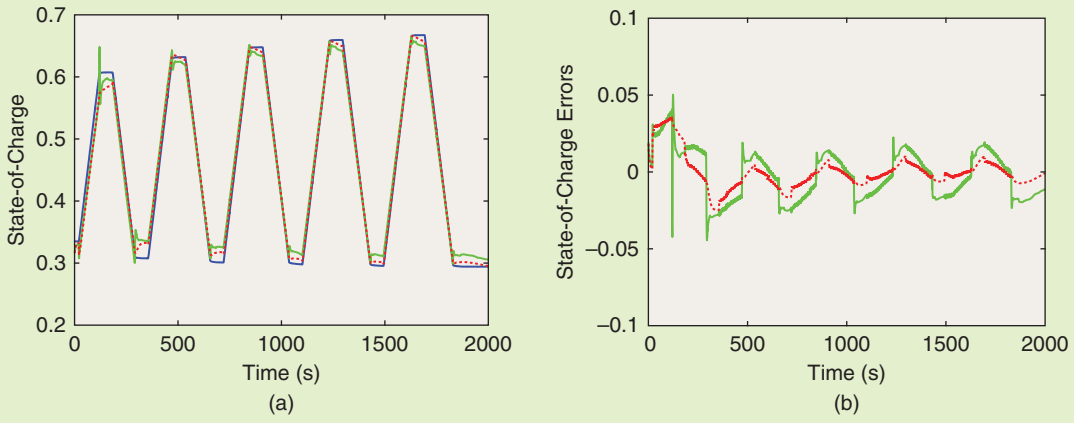

FIGURE 13 A comparison of the enhanced extended Kalman filter (EKF) and the joint EKF using experimental data. (a) Blue line: true state-of-charge (SoC) from the Coulomb counting; green line: joint EKF; red dashed line: enhanced EKF. (b) SoC estimation error; green line: joint EKF; red dashed line: enhanced EKF.

Figure 7 plots the condition number of the observability matrix when the eighth-order augmented model (8) is excited by a constant current. The observability matrix is nonsingular but ill-conditioned, which implies that the eighth-order augmented model (8) is weakly observable. The tuning difficulty of the joint EKF can be explained by the fact that the full-state estimation performance can be dramatically compromised by the existence of weakly observable modes [23], [50]. Even for a strongly observable nonlinear system, EKF tuning may be difficult. Meanwhile, adaptive EKFs, which attempt to alleviate the amount of tuning needed by using online identification of noise covariance matrices, have also been intensively investigated [50]–[52]. Such methods can incur a significantly increased computation load, making their practical utility in BMSs uncertain.

Performance of the EKF heavily depends on matrices Q, R, and P_0. For linear systems, ideally, Q, R, and P_0 are the covariances of the process noise, measurement noise, and initial state error. For nonlinear systems, the tuning of Q, R, and P_0 is not straightforward and typically resorts to the trial-and-error approach, though the existing work does establish some useful insights [53], [54]. A general tuning guideline is that Q and R should take into account the linearization errors as well as noise [53]. Next, the tuning practice followed in the simulation is shown. Denote a constant matrix $Q = \text{diag}\{q^1,\ldots,q^8\}$. Guidelines to determine Q and R are illustrated by exemplifying the determination of q^1, q^8, and R from the first state equation, the eighth state equation, and the output equation of battery model (8). Assume that the noise covariance of the current source is $W_1^x = 10^{-4}$. Considering

$$\begin{aligned}\hat{x}_{k\,|\,k}^1 &= \hat{x}_{k\,|\,k-1}^1 + K_k^1(y_k - \hat{y}_{k\,|\,k-1}) \\ &\approx -\hat{\alpha}_{k-1\,|\,k-1} I_k + \sqrt{q^1} + K^1(y_k - \hat{y}_{k\,|\,k-1}),\end{aligned}$$

with K_k^1 the gain, and the true dynamics $x_k^1 = -\alpha_k(I_k + w_k^1)$, gives

$$x_k^1 - \hat{x}_{k\,|\,k}^1 \approx -K_k^1(y_k - \hat{y}_{k\,|\,k-1}) - \underbrace{[(\alpha_k - \hat{\alpha}_{k-1\,|\,k-1})I_k + \alpha_k w_k^1]}_{d_k^1} - \sqrt{q^1}.$$

Let $q^1 = E[(d_k^1)^2]$ to compensate for linearization errors and noise such that $E[x_k^1 - \hat{x}_{k\,|\,k}^1] = -K_k^1(y_k - \hat{y}_{k\,|\,k-1})$. Considering that $(\alpha_k - \hat{\alpha}_{k-1\,|\,k-1}) \sim 10^{-5}$, $w_k^1 \sim 10^{-2}$, $I_k \sim 10$, the covariance of d_k^1 is on the order of 10^{-8}. Hence, q^1 should take a value around 10^{-8}. Conditions on q^2 and q^3 can also be similarly derived. On the other hand, $q^4,\ldots,q^8$ are associated with parameter dynamics $\theta_{k+1}^i = \theta_k^i + w_k^i$, which are not subject to a linearization error. For $4 \le i \le 8$, q^i depends on the nominal value of the parameter θ^i and how fast the parameter changes. Taking θ^5 as an example, its nominal value is around 10^{-3}. Assume that parameter θ^5 changes at a time constant of about 100 s. Given the sampling period $T_s = 1$ s, the goal is to tune q^8 so that the EKF can track the parameter within its time constant. That is to say, q^8 should be on the order of 10^{-10}. Similar ideas are applicable to tune $q^4,\ldots,q^7$.

The matrix R accounts for uncertainties in $y_k - \hat{y}_{k\,|\,k-1}$, namely, the linearization error and noises. Assume that the voltage sensor has a noise covariance 10^{-6}. With the Taylor-series expansion of $h(x^1)$, uncertainties in $y_k - \hat{y}_{k\,|\,k-1}$ are approximated as

$$\left.\frac{\partial^2 h(x^1)}{\partial (x^1)^2}\right|_{\hat{x}_{k\,|\,k-1}^1} (x_k^1 - \hat{x}_{k\,|\,k-1}^1)^2 - (R_s)_k w_k^1 + v_k + O((x_k^1 - \hat{x}_{k\,|\,k-1}^1)^2).$$

The first term is approximately of the same order as $(x_k^1 - \hat{x}_{k\,|\,k-1}^1)^2$ or 10^{-2}. Given $R_s \sim 10^{-3}$, $w_k^1 \sim 10^{-2}$, and $v_k \sim 10^{-3}$, the second and third terms are on the order of 10^{-5} and 10^{-3}, respectively. Overall, the order of the linearization error is 10^{-2}. This implies that R should be around 10^{-4}. Note that the above selection for Q and R is a worst-case design. In fact, as the EKF estimator converges, the linearization error decreases, which calls for a decline of Q and R accordingly. In the simulation, the matrices Q and R are set

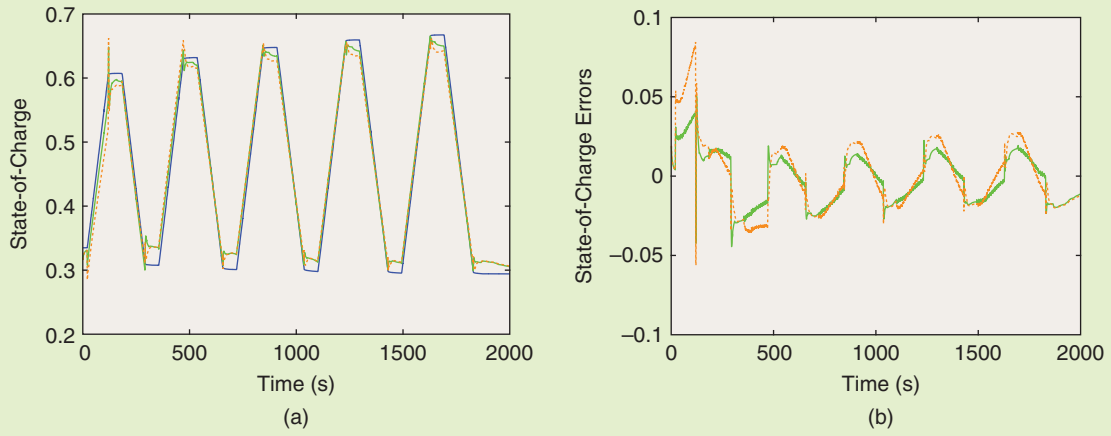

FIGURE 14 A comparison of the two-stage extended Kalman filter (EKF) and the joint EKF using experimental data. (a) Blue solid line: true state-of-charge (SoC) from the Coulomb counting; green solid line: joint EKF; orange dashed line: two-stage EKF. (b) SoC estimation error; green solid line: joint EKF; orange dashed line: two-stage EKF.

to be constant for simplicity. A similar tuning technique has been developed and used to tune the EKF for chemical processes [55].

Two-Stage Extended Kalman Filter Approach

A two-stage EKF based on the optimal two-stage KF (OTSKF) [56], [57] is designed and validated for the adaptive SoC estimation, aiming at balancing the computation complexity and estimation performance. The two-stage EKF is applied to the augmented battery model (8). See "Two-Stage Extended Kalman Filter" for a detailed design of the two-stage EKF for a nonlinear system.

With the same ICs and tuning parameters, both the two-stage and joint EKFs are validated using experimental data. The SoC estimation results are plotted in Figure 14, where the two-stage EKF produces performance comparable to the joint EKF. The computational burden of the two-stage EKF and the joint EKF for the adaptive SoC estimation problem can be evaluated as in [56] and [57]. Given that the dimensions of the state, parameter, input, and output are $n_x = 3$, $n_\theta = 5$, $n_u = 1$, and $n_y = 1$, respectively, the two-stage EKF takes 558 fewer arithmetic operations per sample time than the joint EKF.

Sensitivity Analysis

When addressing an adaptive estimation problem, two important questions to ask are whether adaptive estimation is possible and how difficult it is. These questions can be answered by rigorous observability/identifiability analysis, which has been carried out in different ways. As a standard approach, the observability analysis can be performed on the augmented model (8). Provided that the observability matrix is nonsingular and well-conditioned, stable adaptive SoC estimation is possible [58, Lem. 2.2.4]. When the augmented model (8) is subject to a constant current input, the observability matrix Q_o is nonsingular but ill-conditioned, as shown in Figure 7. To determine which parameter causes the ill-conditioning of Q_o, augment battery model (3) with different parameters and then examine the condition numbers of the augmented battery models. This procedure is tedious because it requires an exhaustive enumeration of all possible parameter sets, and the matrix Q_o is rather intricate. See [59] for an example of applying rigorous algebraic identifiability conditions to an HIV/AIDS model.

Another approach makes use of the sensitivity analysis to determine whether parameter variations can propagate to the output y. Sensitivity analysis is the study of how change in the model output can be apportioned to different sources of change in the model input [60]. Its successful application stretches across many engineering problems, for instance, identifying critical regions in the parameter space [60] or determining the most identifiable subset of parameters to facilitate model reduction and parameter estimation. Particularly, a multitude of recent studies report how sensitivity analysis is used to choose the most significant parameters for diverse engineering systems, for example, in waste-water treatment processes [61]–[63], the activated sludge model [64], and synchronous generators [65], [66]. See [60] for more information about sensitivity theory and applications. Compared with observability analysis, sensitivity analysis is straightforward to troubleshoot an ill-posed estimation problem and thus is instructive in practice.

Sensitivity analysis can be employed to establish that the adaptive SoC estimation based on the augmented model (8) suffers from a fundamental limitation caused by the overparameterized battery model and limited data. Sensitivity analysis can further provide guidelines to bypass this limitation. For simplicity, local sensitivity analysis is performed, where small perturbations of parameters at specified nominal values are first assumed, and then the impact of the

perturbations on the output is quantified [60], [63]. Regarding the augmented model (8), the sensitivity of y with respect to the parameters can be derived

$$\begin{aligned}
&\frac{\partial y}{\partial \theta^1} = \frac{\partial h}{\partial x^1}\frac{\partial x^1}{\partial \theta^1} = -I\frac{\partial h}{\partial x^1},\\
&\frac{\partial y}{\partial \theta^2} = -\frac{\partial x^2}{\partial \theta^2} = -x^2,\\
&\frac{\partial y}{\partial \theta^3} = -\frac{\partial x^2}{\partial \theta^3} = -I,\\
&\frac{\partial y}{\partial \theta^4} = \frac{\partial x^3}{\partial \theta^4} = |I|(\theta^4)^{|I|-1}[x^3 + \operatorname{sign}(I)(1-x^1)s],\\
&\frac{\partial y}{\partial \theta^5} = -I.
\end{aligned} \tag{9}$$

Provided that $x^2 \ll 1, x^3 \ll 1, \theta^4 \approx 1$, and $s = 0.0755$, θ^2 and θ^4 barely affect y and are difficult to identify. This qualitative reasoning is affirmed by the simulation results shown in Figure 15. Since the sensitivities of y with respect to θ^3 and θ^5 are equal to $-I$, Figure 15 only plots $\partial y/\partial \theta^1$, $\partial y/\partial \theta^2$, and $\partial y/\partial \theta^4$, when battery model (3) is subject to the pulse and the UDDS currents.

The above sensitivity analysis result can be nicely interpreted in the adaptive framework [15]. Considering that the gain from the control input to x^1 is $1/(3600C_0) \ll 1$, the state x^1 can be treated as a constant for a reasonably long time interval. Additionally, states x^2 and x^3 always stay in a small neighborhood of the origin. Within a reasonably long time interval, the battery state barely changes, and thus battery model (8) can be treated as an LTI system. With this in mind, a connection between the sensitivity analysis result and the persistent excitation condition can be established [15]. This connection is elucidated by studying a SISO LTI system (6), where A_ζ, B_ζ, and C_ζ are unknown matrices. It is understood that system (6) can be transformed into the form

$$\begin{aligned}
\dot{x} &= Kx + B_y y + B_u u,\\
y &= Cx,
\end{aligned} \tag{10}$$

where both K and C are known and have special structure [15]. Unknown parameters of (10) only appear in B_y and B_u. A set of filters can be constructed to generate known signals $\psi(t)$ such that y takes a linear parameterization [15] $y(t) = \psi(t)\theta$, where $\theta = [B_y^\top, B_u^\top]^\top$ and $\psi(t) = [\psi^1(t), \ldots, \psi^{2n}]$. Applying local sensitivity analysis gives $\partial y(t)/\partial \theta^i = \psi^i(t)$. Thus, parameter θ^i is deemed critical only if the auxiliary signal $\psi^i(t)$ has a relatively large magnitude over $t \in [0, \infty)$. On the other hand, the persistent excitation condition requires there exist constants $0 < T < \infty$ and $0 < \alpha < \beta < \infty$ such that $\alpha \mathbf{I}_{2n} \le \int_t^{t+T} \psi^\top(\tau)\psi(\tau)\,d\tau \le \beta \mathbf{I}_{2n}$.

Sensitivity Analysis-Based Extended Kalman Filter Approach

An enhanced adaptive SoC estimation scheme is provided to reduce the tuning work associated with the joint EKF. As

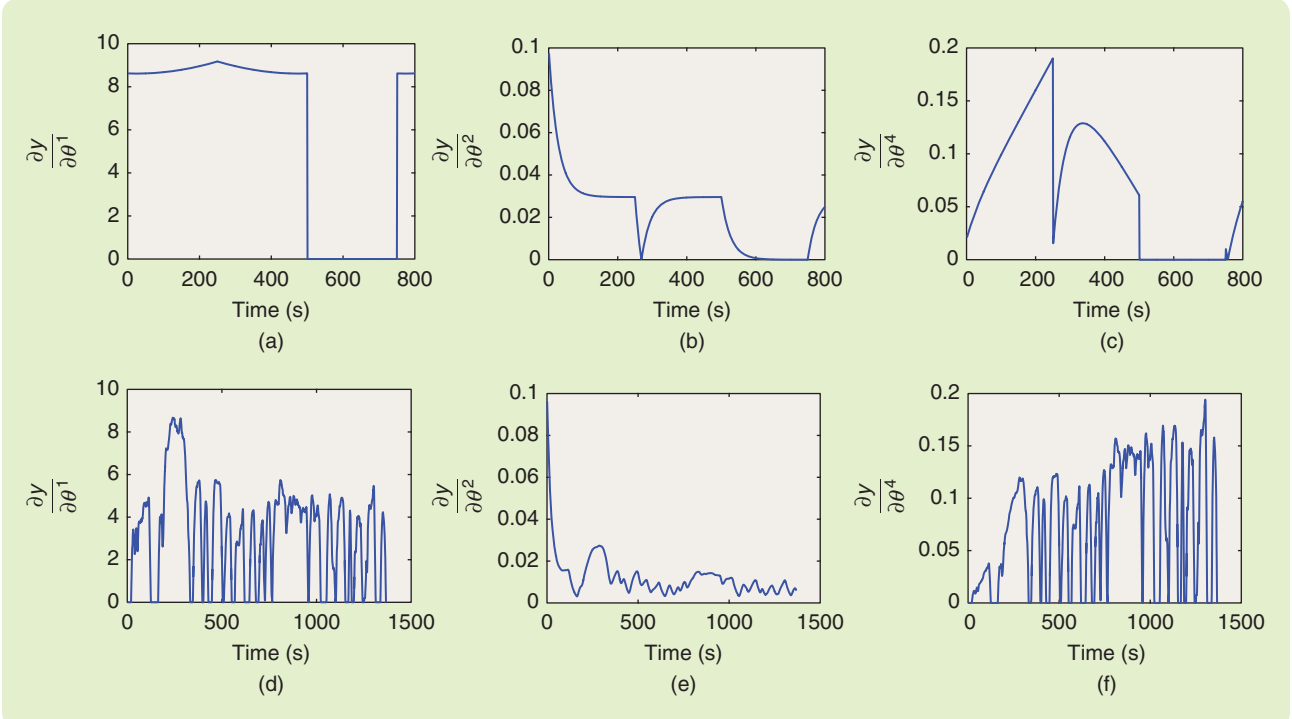

FIGURE 15 Simulation results of sensitivity analysis: $\partial y/\partial \theta^1, \partial y/\partial \theta^2$, and $\partial y/\partial \theta^4$ when battery model (3) is subject to the pulse current and the urban dynamometer driving schedule (UDDS) current, respectively. (a)–(c) Pulse current and (d)–(f) UDDS current. (a) $\partial y/\partial \theta^1$. (b) $\partial y/\partial \theta^2$. (c) $\partial y/\partial \theta^4$. (d) $\partial y/\partial \theta^1$. (e) $\partial y/\partial \theta^2$. (f) $\partial y/\partial \theta^4$.

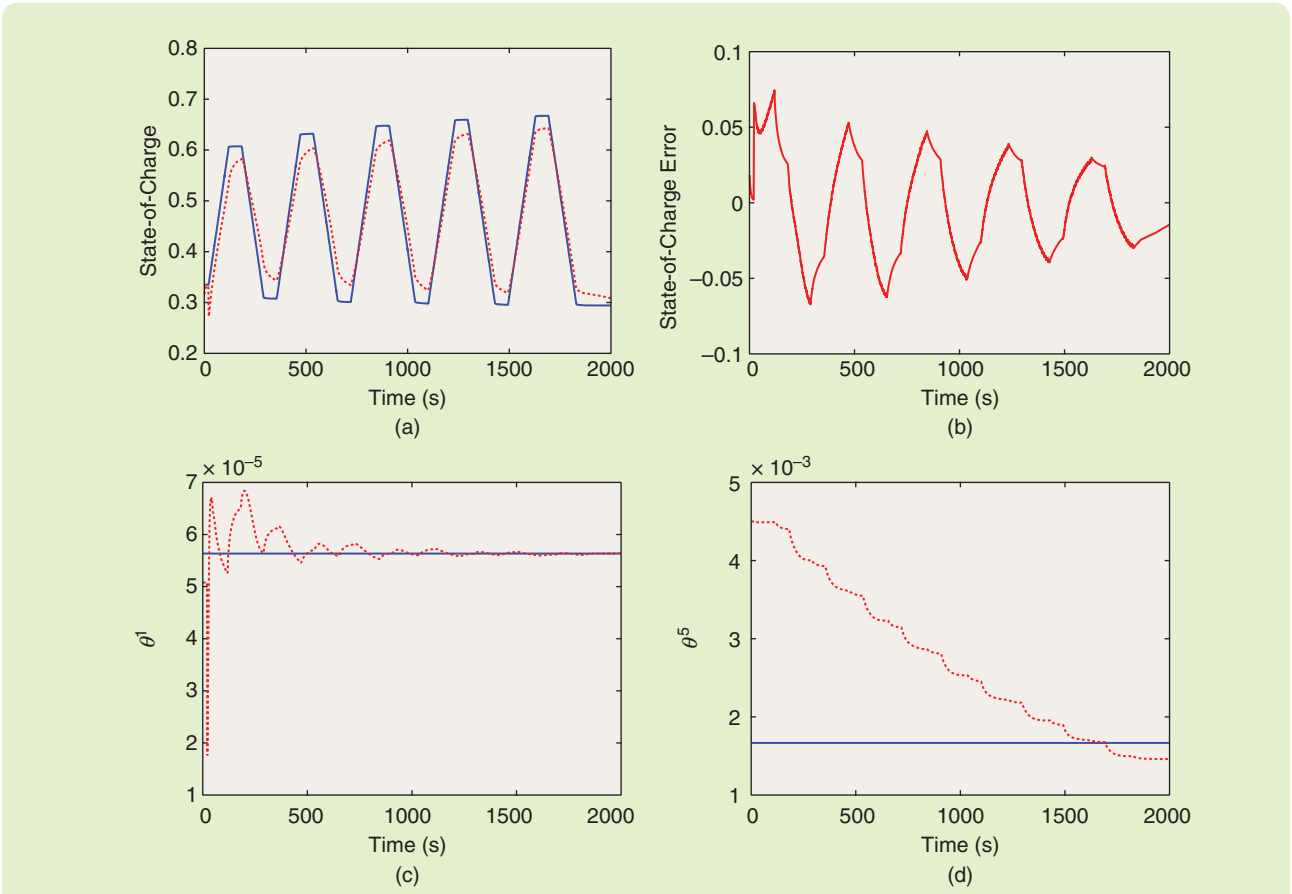

FIGURE 16 A validation of EKF-A using experimental data. (a) Blue line: true state-of-charge (SoC) from the Coulomb counting; red dashed line: estimated. (b) SoC estimation error. (c) Blue line: nominal θ^1; red dashed line: estimated. (d) Blue line: nominal θ^5; red dashed line: estimated.

a direct application of the sensitivity analysis, select a subset of parameters to which the output is strongly sensitive, and then augment battery model (3) with the selected parameters instead of the entire set of parameters. With the most easily identifiable parameters to estimate, the conditions that result from the sensitivity analysis are more likely satisfied. The scheme is also validated by performing the observability analysis on the fourth-order battery model, which is obtained from augmenting battery model (3) with an additional state α. With a constant current applied to the fourth-order battery model, the condition number of the observability matrix is shown in Figure 7. Compared with the eighth-order augmented model, the observability matrix is significantly better conditioned.

This enhanced scheme is validated by conducting two studies based on the experimental data. In the first study, a reduced-order EKF-A is implemented to estimate the battery state x and two parameters θ^1 and θ^5; results are shown in Figure 16. As anticipated, tuning of EKF-A is much more straightforward. The EKF-A provides more consistent estimation of θ^1 and θ^5 than the joint EKF. However, the SoC estimation produced by EKF-A is less accurate than the joint EKF case. With an averaging window size of 1000 time steps, EKF-A outputs parameter estimates: $\hat{\theta}_1 = 5.719 \times 10^{-5}$ and $\hat{\theta}_5 = 7.634 \times 10^{-4}$.

In the second study, a reduced-order EKF-B is used to estimate the battery state and parameters $\theta^2, \theta^3, \theta^4$. Experimental results of EKF-B are given in Figure 17, from which the following facts are observed:

- The SoC estimation from EKF-B is not satisfactory. This is associated with the use of the incorrect maximum capacity value.
- The SoC estimation accuracy of EKF-B is dominated by the error between the α value used in EKF-B and the true value.
- The unknown parameters θ^2, θ^3, and θ^4 are still difficult to identify. This phenomenon is caused by their weak identifiability and agrees with the sensitivity analysis results.

With this analysis and validation, the sensitivity-analysis-based enhanced adaptive SoC estimation scheme is the following:

- Initially, EKF-A estimates the battery state and two parameters θ^1 and θ^5.

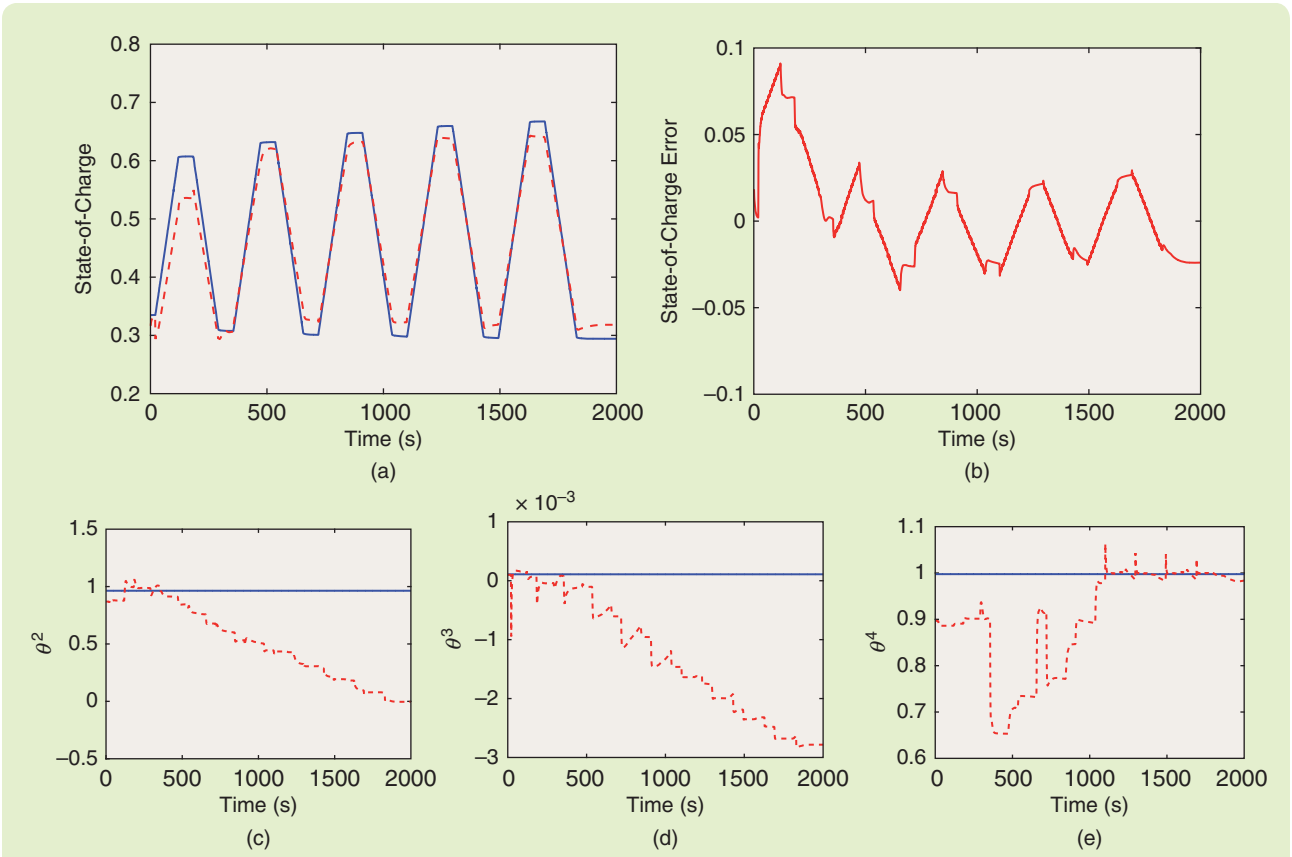

FIGURE 17 A validation of EKF-B using experimental data. (a) Blue line: true state-of-charge (SoC) from the Coulomb counting; red dashed line: estimated. (b) The SoC estimation error. (c) Blue line: nominal θ^2; red dashed line: estimated. (d) Blue line: nominal θ^3; red dashed line: estimated θ^3. (e) Blue line: nominal θ^4; red dashed line: estimated θ^4.

- After EKF-A produces convergent parameter estimates, EKF-B estimates the battery state and the remaining parameters, using θ^1 and θ^5 from EKF-A. The SoC produced by EKF-B constitutes the final SoC estimate.
- Both EKF-A and EKF-B run in the cascade mode. Specifically, EKF-B runs with the sampling period $T_s = 1\,\text{s}$, and EKF-A runs at a much slower time scale compared with EKF-B. This arrangement is justified by the fact that both θ^1 and parameter θ^5 change at a pace much smaller than T_s.

The experimental data are applied to validate the enhanced adaptive SoC estimation scheme, and results are compared with the joint EKF case. As shown in Figure 13, the SoC estimation error of the enhanced adaptive scheme is about $\pm 1\%$ versus $\pm 2\%$ for the joint EKF case. Additionally, the enhanced adaptive scheme enjoys advantages including a reduced level of effort in tuning the resultant EKFs and a lower computational burden.

One of the challenges that a real BMS faces is how to mitigate the adverse effects resulting from variations of the ambient temperature. This is important because the ambient temperature can change the noise properties and battery model parameters. An ideal SoC estimator can either adapt to or reject the fluctuation of the ambient temperature. Improving the enhanced EKF by adapting Q and R to the ambient temperature can be part of the future work.

CONCLUSION AND FUTURE WORK

This article offered an in-depth case study of nonlinear SoC estimation for Li^+ battery management. SoC monitoring is at the heart of an advanced BMS to ensure safe and high-performing operation of Li^+ batteries. This article demonstrated how the celebrated EKF technique can be effectively applied to solve the SoC estimation problem and how fundamental concepts in nonlinear estimation theory can be used to enable the estimator design and interpret the estimation results.

This article performed a thorough observability and sensitivity analysis with a simple ECM battery model, which serves as a backbone for developing effective solutions to SoC estimation. An existing joint EKF-based adaptive SoC estimator, which performs simultaneous state and parameter estimation, is capable of producing accurate SoC estimation but suffers from being difficult to tune and having a relatively high computational cost. The tuning difficulty is, in

large part, due to fundamental limitations originating from the overparameterized battery model and the limited data. Inspired by this analysis, this article further presented two custom EKFs, an enhanced EKF and a two-stage EKF, for adaptive SoC estimation. Compared with the joint EKF, the enhanced EKF has improved estimation accuracy, reduced tuning efforts, and a lower computational burden. The two-stage EKF shows comparable estimation performance but requires considerably less computation. This article presents a systematic observability and sensitivity analysis, revealing and overcoming the potential pitfalls that can undermine a successful application of EKF to SoC estimation.

Despite the success of EKF-based techniques in the SoC estimation, a few questions still remain open, which may represent opportunities for further investigation. The first is how to prove the convergence properties of the SoC estimators. While there exist some results about the convergence of EKF, they have not yet been effectively transitioned to SoC estimation. Most nonlinear SoC observers also lack convergence analysis because the battery models usually do not admit the special structures often needed for the relevant proofs. Second, the full-state estimation pursued in the existing works is indeed unnecessary since not every state or parameter will be of interest or use to the BMS. Thus, a key question is how to construct reduced-order estimators or functional observers for higher computational accuracy. Third, going beyond the cell level, is how to perform SoC monitoring and tracking for Li^+ battery packs. SoC estimation at the pack level is rendered more challenging and interesting by the increased system sophistication and mutual cell-to-cell influence. Along these lines, how to make the best use of the battery dynamics to reduce the number of voltage and current sensors without a significant sacrifice of estimation accuracy is an interesting problem.

AUTHOR INFORMATION

Yebin Wang (yebinwang@ieee.org) is a senior principal research scientist at Mitsubishi Electric Research Laboratories in Cambridge, Massachusetts. He received the B.Eng. degree in mechatronics engineering from Zhejiang University, Hangzhou, China, in 1997, the M.Eng. degree in control theory and control engineering from Tsinghua University, Beijing, China, in 2001, and the Ph.D. degree in electrical engineering from the University of Alberta, Edmonton, Canada, in 2008. His research interests include nonlinear control and estimation, optimal control, and adaptive systems and their applications including mechatronic systems. He was a software engineer, project manager, and manager of R&D in industry in Beijing, China. He can be contacted at Mitsubishi Electric Research Laboratories, 201 Broadway, Cambridge, Massachusetts 02139, USA.

Huazhen Fang is an assistant professor in the Department of Mechanical Engineering at the University of Kansas. His broad research interest lies in dynamic systems and control, with a current application focus on advanced battery management. He received the Ph.D. degree in mechanical engineering in 2014 from the Department of Mechanical and Aerospace Engineering, University of California, San Diego. He received the M.Sc. degree in mechanical engineering from the University of Saskatchewan, Saskatoon, Canada, in 2009 and the B.Eng. degree in computer science and technology from Northwestern Polytechnic University, Xi'an, China, in 2006.

Lei Zhou received the B.S. degree from the Department of Precision Instrument and Mechanology, Tsinghua University, China, in 2012 and received S.M. degree from the Department of Mechanical Engineering, Massachusetts Institute of Technology (MIT), in 2014. She is currently working toward the Ph.D. degree in the Department of Mechanical Engineering at MIT. Her research interests include control, estimation, and precision mechatronics.

Toshihiro Wada received the B.Eng. degree in informatics and mathematical science and the M. Informatics degree in applied analysis and complex dynamical systems from Kyoto University, Japan, in 2005 and 2007, respectively. His current research interests include sensing and optimization of battery systems.

REFERENCES

[1] J.-M. Tarascon and M. Armand, "Issues and challenges facing rechargeable lithium batteries," *Nature*, vol. 414, pp. 359–367, Nov. 2001.

[2] M. Doyle, T. F. Fuller, and J. Newman, "Modeling of galvanostatic charge and discharge of the lithium/polymer/insertion cell," *J. Electrochem. Soc.*, vol. 140, no. 6, pp. 1526–1533, 1993.

[3] C. Y. Wang, W. B. Gu, and B. Y. Liaw, "Micro-macrosopic coupled modeling of batteries and fuel cells I. model development," *J. Electrochem. Soc.*, vol. 145, no. 10, pp. 3407–3417, 1998.

[4] R. Rao, S. Vrudhula, and D. N. Rakhmatov, "Battery modeling for energy-aware system design," *Computer*, vol. 36, no. 12, pp. 77–87, Dec. 2003.

[5] S. Santhanagopalan, Q. Guo, P. Ramadass, and R. E. White, "Review of models for predicting the cycling performance of lithium ion batteries," *J. Power Sources*, vol. 156, no. 2, pp. 620–628, 2006.

[6] G. L. Plett, "Extended Kalman filtering for battery management systems of LiPB-based HEV battery packs: Part 2. Modeling and identification," *J. Power Sources*, vol. 134, no. 2, pp. 262–276, 2004.

[7] M. Chen and G. A. Rincón-Mora, "Accurate electrical battery model capable of predicting runtime and I-V performance," *IEEE Trans. Energy Convers.*, vol. 31, no. 2, pp. 504–511, June 2006.

[8] N. Chaturvedi, R. Klein, J. Christensen, J. Ahmed, and A. Kojic, "Algorithms for advanced battery-management systems," *IEEE Contr. Syst. Mag.*, vol. 30, no. 3, pp. 49–68, 2010.

[9] T. F. Fuller, M. Doyle, and J. Newman, "Simulation and optimization of the dual lithium ion insertion cell," *J. Electrochem. Soc.*, vol. 141, no. 1, pp. 1–10, 1994.

[10] S. Atlung, K. West, and T. Jacobsen, "Dynamic aspects of solid solution cathodes for electrochemical power sources," *J. Electrochem. Soc.*, vol. 126, no. 8, pp. 1311–1321, 1979.

[11] S. K. Rahimian, S. Rayman, and R. E. White, "Extension of physics-based single particle model for higher charge-discharge rates," *J. Power Sources*, vol. 224, pp. 180–194, 2013.

[12] Y.-S. Lee and M.-W. Cheng, "Intelligent control battery equalization for series connected lithium-ion battery strings," *IEEE Trans. Ind. Electron.*, vol. 52, no. 5, pp. 1297–1307, Oct. 2005.

[13] H. He, R. Xiong, and J. Fan, "Evaluation of lithium-ion battery equivalent circuit models for state of charge estimation by an experimental approach," *Energies*, vol. 4, pp. 582–598, 2011.

[14] Y. Hu, S. Li, and H. Peng, "A comparative study of equivalent circuit models for Li-ion batteries," *J. Power Sources*, vol. 198, pp. 359–367, Jan. 2012.

[15] K. S. Narendra and A. M. Annaswamy, *Stable Adaptive Systems*. Englewood Cliffs, NJ: Prentice Hall, 1989.

[16] T. Kim, Y. Wang, Z. Sahinoglu, T. Wada, and S. Hara, "Model-based condition monitoring for lithium-ion batteries," *J. Power Sources*, vol. 295, pp. 16–27, Nov. 2015.
[17] H. Fang, Y. Wang, Z. Sahinoglu, T. Wada, and S. Hara, "Adaptive estimation of state of charge for lithium-ion batteries," in *Proc. American Control Conf.*, 2013, pp. 3485–3491.
[18] R. Marino and P. Tomei, *Nonlinear Control Design: Geometric, Adaptive, and Robust*. Hertfordshire, U.K.: Prentice Hall, 1995.
[19] J. P. Gauthier, H. Hammouri, and S. Othman, "A simple observer for nonlinear systems–applications to bioreactors," *IEEE Trans. Automat. Control*, vol. 37, no. 6, pp. 875–880, June 1992.
[20] J. P. Gauthier and I. A. K. Kupka, "Observability and observers for nonlinear systems," *SIAM J. Control Optim.*, vol. 32, no. 4, pp. 975–994, July 1994.
[21] H. Nijmeijer and A. J. van der Schaft, *Nonlinear Dynamical Control Systems*. New York: Springer-Verlag, 1990.
[22] E. Busvelle and J. P. Gauthier, "High-gain and non-high-gain observers for nonlinear systems," in *Proc. Contemporary Trends in Nonlinear Geometric Control Theory*, 2002, pp. 257–286.
[23] J. A. Farrell and M. Barth, *The Global Positioning System and Inertial Navigation*. New York: McGraw-Hill, 1998.
[24] R. Rajamani, "Observers for Lipschitz nonlinear systems," *IEEE Trans. Automat. Control*, vol. 43, no. 3, pp. 397–401, Mar. 1998.
[25] K. R. Shouse and D. G. Taylor, "Discrete-time observers for singularly perturbed continuous-time systems," *IEEE Trans. Automat. Control*, vol. 40, no. 2, pp. 224–235, Feb. 1995.
[26] G. H. Golub and C. F. Van Loan, *Matrix Computation*. Baltimore: JHU Press, 2012.
[27] J. P. Hespanha, D. Liberzon, D. Angeli, and E. D. Sontag, "Nonlinear norm-observability notations and stability of switched systems," *IEEE Trans. Automat. Control*, vol. 50, no. 2, pp. 154–168, Feb. 2005.
[28] A. J. Krener and A. Isidori, "Linearization by output injection and nonlinear observers," *Syst. Control Lett.*, vol. 3, no. 1, pp. 47–52, June 1983.
[29] A. J. Krener and W. Respondek, "Nonlinear observers with linearizable error dynamics," *SIAM J. Control Optim.*, vol. 23, no. 2, pp. 197–216, Mar. 1985.
[30] J. Rudolph and M. Zeitz, "Block triangular nonlinear observer normal form," *Syst. Control Lett.*, vol. 23, no. 1, pp. 1–8, July 1994.
[31] W. Respondek, A. Pogromsky, and H. Nijmeijer, "Time scaling for observer design with linearizable error dynamics," *Automatica*, vol. 40, no. 2, pp. 277–285, Feb. 2004.
[32] Y. Wang and A. Lynch, "A block triangular observer forms for nonlinear observer design," *Int. J. Control*, vol. 81, no. 2, pp. 177–188, 2008.
[33] G. Zheng, D. Boutat, and J. Barbot, "Single output dependent observability normal form," *SIAM J. Control Optim.*, vol. 46, no. 6, pp. 2242–2255, 2007.
[34] W. Perruquetti, T. Floquet, and E. Moulav, "Finite-time observers: Application to secure communication," *IEEE Trans. Automat. Control*, vol. 53, no. 2, pp. 356–360, Feb. 2008.
[35] J. H. Ahrens and H. K. Khalil, "High-gain observers in the presence of measurement noise: A switched-gain approach," *Automatica*, vol. 45, no. 4, pp. 936–943, Apr. 2009.
[36] Y. Wang and A. F. Lynch, "Multiple time scalings of a multi-output observer form," *IEEE Trans. Automat. Control*, vol. 55, no. 4, pp. 966–971, Apr. 2010.
[37] S. Julier, J. Uhlmann, and H. Durrant-Whyte, "A new approach for filtering nonlinear systems," in *Proc. American Control Conf.*, 1995, vol. 3, pp. 1628–1632.
[38] S. J. Julier and J. K. Uhlmann, "A new extension of the Kalman filter to nonlinear systems," in *Proc. AeroSense: The 11th Int. Symp. Aerospace/Defence Sensing, Simulation and Controls*, 1997, pp. 182–193.
[39] G. Evensen, "Sequential data assimilation with a nonlinear quasi-geostrophic model using Monte Carlo methods to forecast error statistics," *J. Geophys. Res.*, vol. 99, no. C5, pp. 10 143–10 162, 1994.
[40] G. Evensen and P. J. van Leeuwen, "Assimilation of geosat altimeter data for the agulhas current using the ensemble Kalman filter with a quasi-geostrophic model," *Mon. Weather Rev.*, vol. 124, pp. 85–96, 1996.
[41] P. L. Houtekamer and H. L. Mitchell, "Data assimilation using an ensemble Kalman filter technique," *Mon. Weather Rev.*, vol. 126, pp. 796–811, 1998.
[42] N. Gordon, D. Salmond, and A. Smith, "Novel approach to nonlinear/non-Gaussian Bayesian state estimation," *IEE Proc. F Radar Signal Process.*, vol. 140, no. 2, pp. 107–113, 1993.
[43] C. Rao, J. Rawlings, and D. Mayne, "Constrained state estimation for nonlinear discrete-time systems: Stability and moving horizon approximations," *IEEE Trans. Automat. Control*, vol. 48, no. 2, pp. 246–258, 2003.
[44] T. Wada, T. Takegami, and Y. Wang, "Sequential estimation of state of charge and equivalent circuit parameters for lithium-ion batteries," in *Proc. American Control Conf.*, Chicago, IL, July 2015, pp. 2494–2498.
[45] A. B. Sripad and D. L. Snyder, "A necessary and sufficient condition for quantization errors to be uniform and white," *IEEE Trans. Acoustics Speech Signal Process.*, vol. ASSP-25, no. 5, pp. 442–448, Oct. 1977.
[46] B. Widrow, I. Kollár, and M.-C. Liu, "Statistical theory of quantization," *IEEE Trans. Instrum. Meas.*, vol. 45, no. 2, pp. 353–351, Apr. 1996.
[47] M. Fu and C. E. de Souza, "State estimation for linear discrete-time systems using quantized measurements," *Automatica*, vol. 45, no. 12, pp. 2937–2945, Dec. 2009.
[48] Woodbank Communications Ltd. Traction batteries for EV and HEV applications [Online]. Available: http://www.mpoweruk.com/traction.htm
[49] G. L. Plett, "Extended Kalman filtering for battery management systems of LiPB-based HEV battery packs: Part 3. State and parameter estimation," *J. Power Sources*, vol. 134, no. 2, pp. 277–292, 2004.
[50] F. V. Lima, M. R. Rajamanni, T. A. Soderstrom, and J. B. Rawlings, "Covariance and state estimation of weakly observable systems: Application to polymerization processes," *IEEE Trans. Contr. Syst. Technol.*, vol. 21, no. 4, pp. 1249–1257, July 2013.
[51] R. K. Mehra, "On the identification of variances and adaptive Kalman filtering," *IEEE Trans. Automat. Control*, vol. AC-15, no. 2, pp. 175–184, 1970.
[52] W. Ding, J. Wang, and C. Rizos, "Improving adaptive Kalman estimation in GPS/INS integration," *J. Navig.*, vol. 60, pp. 517–529, 2007.
[53] B. F. L. Scala, R. Bitmead, and B. G. Quinn, "An extended Kalman filter frequency tracker for high-noise environments," *IEEE Trans. Signal Process.*, vol. 44, no. 3, pp. 431–434, Feb. 1996.
[54] M. Boutayeb and D. Aubry, "A strong tracking extended Kalman observer for nonlinear discrete-time systems," *IEEE Trans. Automat. Control*, vol. 44, no. 8, pp. 1550–1556, Aug. 1999.
[55] J. Valappil and C. Georgakis, "Systematic estimation of the state noise statistics for extended Kalman filters," *AIChE J.*, vol. 46, no. 2, pp. 292–308, 2000.
[56] C.-S. Hsieh and F.-C. Chen, "Optimal solution of the two-stage Kalman estimator," *IEEE Trans. Automat. Control*, vol. 44, no. 1, pp. 194–199, 1999.
[57] M. Hilairet, F. Auger, and E. Berthelot, "Speed and rotor flux estimation of induction machines using a two-stage extended Kalman filter," *Automatica*, vol. 45, no. 8, pp. 1819–1827, 2009.
[58] E. M. Tunali and T. J. Tarn, "New results for identifiability of nonlinear systems," *IEEE Trans. Automat. Control*, vol. AC-32, no. 2, pp. 146–154, Feb. 1987.
[59] X. Xia and C. H. Moog, "Identifiability of nonlinear systems with applications to HIV/AIDS models," *IEEE Trans. Automat. Control*, vol. 48, no. 2, pp. 330–336, Feb. 2003.
[60] A. Saltelli, M. Ratto, T. Andres, F. Campolongo, J. Cariboni, D. Gatelli, M. Saisana, and S. Tarantola, *Global Sensitivity Analysis: The Primer*. Hoboken, NJ: Wiley, 2008.
[61] N. A. Noykova and M. Gyllenberg, "Sensitivity analysis and parameter estimation in a model of anaerobic waste water treatment processes with substrate inhibition," *Bioprocess Eng.*, vol. 23, no. 4, pp. 343–349, 2000.
[62] T. G. Müller, N. Noykova, M. Gyllenberg, and J. Timmer, "Practical identification in dynamical models of anerobic waste water treatment," *Math. Biosci.*, vol. 177, pp. 147–160, 2002.
[63] A. van Griensven, T. Meixner, S. Grunwald, T. Bishop, M. Diluzio, and R. Srinivasan, "A global sensitivity analysis tool for the parameters of multi-variable catchment models," *J. Hydrol.*, vol. 324, pp. 10–23, 2006.
[64] R. Brun, M. Kühni, H. Siegrist, W. Gujer, and P. Reichert, "Practical identifiability of ASM2d parameters-systematic selection and tuning of parameter subsets," *Water Res.*, vol. 36, no. 16, pp. 4113–4127, 2002.
[65] M. Burth, G. C. Verghese, and M. Velez-Reyes, "Subset selection for improved parameter estimation in on-line identification of a synchronous generator," *IEEE Trans. Power Syst.*, vol. 14, no. 1, pp. 218–225, Feb. 1999.
[66] C. E. Nino and M. Velez-Reyes, "Dealing with ill conditioning in recursive parameter estimation for a synchronous generator," in *Proc. 32nd Annu. Conf. IEEE Industrial Electronics Society*, Paris, France, Nov. 2006, pp. 1089–1094.